Endoglin, a novel biomarker and therapeutical target to prevent malignant peripheral nerve sheath tumor growth and metastasis

Teresa González-Muñoz[1], Angela Di Giannatale[2], Susana García-Silva[1], Vanesa Santos[1], Sara Sánchez-Redondo[1], Claudia Savini[3], Osvaldo Graña-Castro[4], Carmen Blanco-Aparicio[5], Suzanne Fischer[6,7], Olivier De Wever[6,7], Edgar Creus-Bachiller[8,8b], Sara Ortega-Bertran[8,8b], David J Pisapia[9,10], Jose L Rodríguez-Peralto[11], Juana Fernández-Rodríguez[8, 8b, ,8c,8d], Cleofé Romagosa Pérez-Portabella[12], Rita Alaggio[11], Maria Serena Benassi[13], Laura Pazzaglia[13, 14], Katia Scotlandi[13], Nancy Ratner[15], Kaleb Yohay[16], Charles P. Theuer[17] and Héctor Peinado[1#].

Affiliations

[1] Microenvironment and Metastasis Laboratory, Molecular Oncology Programme, Spanish National Cancer Research Center (CNIO), Madrid, Spain.

[2] Department of Hematology and Oncology, Cell and Gene Therapy, Bambino Gesù Children's Hospital, IRCCS, Rome, Italy.

[3] Patients in Science, medical writing and communication, Valencia, Spain.

[4] Bioinformatics Unit, Structural Biology Programme, Spanish National Cancer Research Centre (CNIO), Madrid, Spain. Current address: Institute of Applied Molecular Medicine (IMMA-Nemesio Díez), Department of Basic Medical Sciences, School of Medicine, San Pablo-CEU University, CEU Universities, Boadilla del Monte, Madrid, Spain.

[5] Experimental Therapeutics Program, Spanish National Cancer Research Centre (CNIO), C/Melchor Fernández Almagro 3, Madrid, Spain.

[6] Laboratory of Experimental Cancer Research, Cancer Research Institute Ghent, Ghent, Belgium.

[7] Department of Human Structure and Repair, Ghent University, Ghent, Belgium.

[8] Hereditary Cancer Program, Catalan Institute of Oncology, Hospitalet de Llobregat, Barcelona, Spain

[8b] Program in Molecular Mechanisms and Experimental Therapy in Oncology (Oncobell), IDIBELL, Hospitalet de Llobregat, Barcelona, Spain

[8c] Centro de Investigación Biomédica en Red de Cáncer (CIBERONC), Spain

[8d] Plataforma Mouse Lab, servicios científico-tècnicos, IDIBELL, l'Hospitalet de Llobregat, Barcelona, Spain

[9] Englander Institute of Precision Medicine, Weill Cornell Medicine, New York, NY, USA.

[10] Department of Pathology and Laboratory Medicine, Weill Cornell Medicine, New York, NY, USA.

[11]Department of Dermatology, 12 de Octubre University hospital, Complutense University of Madrid, Investigation institute I+12, CIBERONC, Madrid, Spain.

[12] Vall de Hebron University Hospital and Autonomous University of Barcelona, Barcelona, Spain.

[13] Laboratory of Experimental Oncology, IRCCS Istituto Ortopedico Rizzoli, Bologna, Italy.

[14] Pathology Unit, Department of Laboratories, Bambino Gesu Children's Hospital, IRCCS, Rome, Italy. Department of Medical-Surgical Sciences and Biotechnologies La Sapienza University, Rome, Italy

[15] Cincinnati Children's Hospital Medical Center, Cincinnati, USA.

[16] New York University Grossman School of Medicine, New York, NY, USA.

[17] TRACON Pharmaceuticals, Inc., San Diego, California, USA.

[#] Corresponding Author: hpeinado@cnio.es, Spanish National Cancer Research Centre (CNIO), Melchor Fernández Almagro, 3, 28029 Madrid, Spain

Running title: Endoglin targeting reduces MPNST growth and metastasis.

Key words: MPNST, angiogenesis, metastasis, endoglin, targeted therapy, combination treatment.

The authors declare that there is no conflict of interest.

ABSTRACT

Purpose: Malignant peripheral nerve sheath tumors (MPNSTs) are highly aggressive soft-tissue sarcomas that lack effective treatments, underscoring the urgent need to uncover novel mediators of MPNST pathogenesis that may serve as potential therapeutic targets. Tumor angiogenesis is considered a critical event in MPNST transformation and progression. Here, we have investigated whether endoglin (ENG), a TGF-β coreceptor with a crucial role in angiogenesis, could be a novel therapeutic target in MPNSTs.

Experimental Design: ENG expression was evaluated in human peripheral nerve sheath tumor tissues and plasma samples. Effects of tumor cell-specific ENG expression on gene expression, signaling pathway activation and *in vivo* MPNST growth and metastasis were investigated. The efficacy of ENG targeting in monotherapy or in combination with MEK inhibition was analyzed in xenograft models.

Results: ENG expression was found to be upregulated in both human MPNST tumor tissues and plasma circulating small extracellular vesicles. We demonstrated that ENG modulates Smad1/5 and MAPK/ERK pathway activation and pro-angiogenic and pro-metastatic gene expression in MPNST cells and plays an active role in tumor growth and metastasis *in vivo*. Targeting with ENG-neutralizing antibodies (TRC105/M1043) decreased MPNST growth and metastasis in xenograft models by reducing tumor cell proliferation and angiogenesis. Moreover, combination of anti-ENG therapy with MEK inhibition effectively reduced tumor cell growth and angiogenesis.

Conclusions: Our data unveil a tumor-promoting function of ENG in MPNSTs and support the use of this protein as a novel biomarker and a promising therapeutic target for this disease.

Statement of translational relevance

Malignant peripheral nerve sheath tumors (MPNSTs) present a poor clinical outcome due to tumor aggressiveness and the absence of effective treatments that underline the need for identifying novel therapeutic approaches. Here, we show that endoglin (ENG) is upregulated in human MPNSTs and we uncover an important role for this coreceptor in MPNST. ENG-neutralizing antibodies (TRC105/M1043) decreased MPNST growth and metastasis in xenograft models. Notably, TRC105 has shown promising efficacy in phase I-III trials involving patients with different solid tumor types, particularly in those with specific soft-tissue sarcoma subtypes. Our data support a novel use of TRC105 for MPNST treatment. Currently, MEK inhibitors are used in the clinic to shrink plexiform neurofibromas; however, preclinical studies have revealed robust yet variable responses to MEK inhibition alone in MPNSTs. Our findings suggest that combination of anti-ENG with MEK inhibition could improve therapeutic efficacy in tumors with limited response to MEK inhibitor monotherapy.

INTRODUCTION

Malignant peripheral nerve sheath tumors (MPNSTs) are highly aggressive soft-tissue sarcomas (STS) derived from cells of the Schwann cell lineage (1). About 40% to 50% of these tumors arise in the context of the genetic disorder neurofibromatosis type 1 (NF1) (2). Indeed, NF1 patients are predisposed to develop benign peripheral nerve sheath tumors (PNSTs), including dermal and plexiform neurofibromas (PNs) (3). However, PNs can undergo malignant transformation, progressing to pre-malignant lesions called atypical neurofibromatous neoplasms of uncertain biological potential (ANNUBPs) and ultimately MPNSTs, a malignant STS with a high mortality rate (3). Another 40% to 47% of MPNSTs are sporadic, and the remaining 10% to 13% occur at sites of prior radiotherapy (2). Irrespective of their origin, these tumors have a strong tendency to relapse and metastasize, with an estimated 5-year survival rate of 15% to 50% (4). Despite this poor prognosis, there is a significant lack of diagnostic biomarkers for early detection of this disease (4). Regarding the treatment, complete surgical resection, which is the only known effective therapy, is often not feasible due to tumor size, location and/or the presence of metastases (5). MPNSTs are relatively refractory to conventional radiation and chemotherapy (5), and targeted therapies have shown limited clinical efficacy in these tumors (6). Therefore, MPNST patients face a significant unmet therapeutic need, highlighting the urgent demand to uncover novel mediators of pathogenesis and new therapeutic targets.

A common event in the pathogenesis of MPNSTs is the biallelic loss of *NF1* gene that encodes the RAS-GTPase activating protein (GAP) neurofibromin, resulting in the hyperactivation of RAS and its downstream signaling pathways (e.g. RAS/MEK/ERK pathway) (3). In fact, MEK inhibition effectively, albeit transiently, inhibited tumor growth in both NF1-associated and sporadic MPNST mouse models (6), supporting the relevance of the RAS/MEK/ERK pathway in MPNST growth. Notably, MEK inhibitors (MEKis) represent the most effective targeted therapy against PNs, recognized precursors of MPNSTs, and indeed the MEKi selumetinib has become the first ever FDA-approved drug for these patients (6). Accordingly, they are being tested in clinical trials for MPNSTs (NCT03433183; NCT05253131). In addition to tumor-cell intrinsic mechanisms, alterations in the tumor microenvironment (TME) are now recognized as critical elements influencing MPNST development (7). Particularly, tumor angiogenesis plays a crucial role in the transformation and progression of MPNSTs (8,9). In fact, increased VEGF expression and vascularization were correlated with tumor malignancy and poor prognosis in MPNST patients (10). A recent phase II trial with the antiangiogenic agent pazopanib demonstrated better outcomes than those achieved with any of the targeted therapies previously tested in MPNST patients, with a clinical benefit rate (CBR) at 12 weeks of 50% (11). In addition, anti-endoglin (ENG) antibody-based therapy using TRC105 has shown promising efficacy in advanced STS subtypes (12-14). Therefore, we postulate that anti-ENG therapies alone or in combination with a MEKi could be a potential new therapeutic approach in MPNSTs.

The TGF-β coreceptor ENG is highly expressed in activated endothelial cells (ECs) and it plays a crucial role in angiogenesis (15). Upon stimulation with ligands (e.g. TGF-β and BMP-9), ENG promotes phosphorylation of downstream Smad1 protein, stimulating EC proliferation and migration (15). Notably, ENG expression has been shown to be upregulated in the vascular endothelium of many solid tumor types, being associated with poor prognosis and metastatic disease (16). ENG is also present at high levels in tumor cells of diverse malignancies, including sarcoma (16,17). In fact, ENG promotes the aggressiveness and tumorigenesis of different sarcoma cell lines, and its overexpression predicts worse outcomes in patients with selective sarcoma subtypes (17). However, the role of ENG in MPNST aggressiveness and its potential as a therapeutic target have not been evaluated.

Here we discovered that ENG is highly expressed in both ECs and tumor cells of human MPNSTs, and its expression correlates with advanced tumor stages (local recurrence and distant metastasis). Moreover, ENG levels were elevated in plasma-circulating small extracellular vesicles (sEVs) from MPNST patients. Mechanistically, we found that ENG expression in MPNST cells regulates Smad1/5 and MAPK/ERK pathway activation driving pro-angiogenic and pro-metastatic gene expression *in vitro,* promoting tumor growth and metastasis *in vivo* as well. Importantly, we reveal that targeting ENG with neutralizing antibodies reduces MPNST tumor growth in xenograft models, by impairing tumor cell proliferation, angiogenesis and ultimately metastasis. Furthermore, the combination of anti-ENG antibodies and the MEKi PD-0325901/Mirdametinib efficiently inhibited both primary tumor growth and metastasis formation. Altogether, our data unveil an important role for ENG in MPNST promoting tumor cell growth, angiogenesis and metastasis and support its use as a promising therapeutic target. Moreover, our findings suggest that the combination of anti-ENG and MEK inhibition could be an attractive approach for the treatment of MPNSTs, mainly for those that exhibit moderate response to MEKi monotherapy.

MATERIALS AND METHODS

Patient samples

Paraffin-embedded PNST tissue samples were collected from four independent patient cohorts at Weill Cornell Medical College (New York, USA), Hospital 12 de Octubre (Madrid, Spain), Bambino Gesù Children's Hospital (Rome, Italy) and Hospital Vall d'Hebron (Barcelona, Spain). The complete collection comprised 39 PNs, 9 ANNUBPs and 38 MPNSTs (24 NF1-associated and 14 sporadic). The tissue microarray (TMA) containing 20 tissue cores retrieved from human primary and local recurrent MPNSTs and lung metastases was obtained from the Hospital Virgen del Rocío (Seville, Spain). Human peripheral blood samples were taken from 32 control healthy subjects and patients with PNs (n=32) and MPNSTs (n=11) at Weill Cornell Medical College, Banco Nacional de ADN Carlos III (Salamanca, Spain) and Instituto Ortopedico Rizzoli (Bologna, Italy), all histologically confirmed. Whole-blood was collected in EDTA tubes, and plasma was isolated by centrifugation at 1,100g for 10min. Patients presenting with a high-grade MPNST (FNCLCC 3) at the outpatient clinic of the Department of Orthopaedic Surgery and Traumatology at Ghent University Hospital, Belgium, were offered to participate in the study of tissue harvesting, storage and establishment of patient-derived cell-lines.

Human studies were approved by the local ethics committees (Instituto de Salud Carlos III, CEI PI13_2015v2, and Ghent University Hospital, Belgium, EC 2018/0080) and were conducted in accordance with the International Conference on Harmonization, Good Clinical Practice guidelines, and the Declaration of Helsinki. All individuals provided written informed consent.

sEV isolation and ELISA analysis of soluble and EV-secreted ENG in plasma samples

Human plasma samples (1 ml) were centrifuged at 3,000g for 20min. The supernatant was further centrifuged at 12,000g for 20min. sEVs were subsequently harvested by centrifugation at 100,000g for 70min. The supernatant (EV-depleted plasma) was kept to quantify soluble ENG concentration. The sEV pellet was washed with PBS and collected by another ultracentrifugation at 100,000g for 70min. All centrifugations were performed at 10ºC using a Beckman Optima X100 centrifuge with a Beckman 50.4 Ti rotor. sEVs were resuspended in PBS and the protein content was measured by Pierce bicinchoninic acid (BCA) assay (Thermo Fisher). Particle concentration was determined using Nanosight Nanoparticle tracking analysis (NTA, Malvern). ENG levels were measured in both sEV-enriched and EV-depleted plasma fractions by ELISA (Abcam, ab100507), following the manufacturer's instructions. For the quantification of sEV-secreted ENG, 5 µg of total sEVs were resuspended in 100 µl of Assay Diluent provided with the kit.

Cell culture

The human NF1-associated MPNST cell lines ST88-14, 90-8, NMS-2, S462 and the sporadic MPNST cell line STS26T were generously provided by Dr. Eduard Serra (Institute for Health Science Research Germans Trias i Pujol, Barcelona, Spain) and Dr. Conxi Lázaro (ICO-IDIBELL, Barcelona, Spain). MPNST-SP-10 cell line was established in the laboratory of Dr. Conxi Lázaro and was derived from a sporadic patient. Genomic and histologic data validated the tumor as an

MPNST (manuscript under preparation). The SNF96.2, SNF02.2 and SNF94.3 cell lines (NF1-derived MPNST) were purchased from ATCC. All these cells were cultured in high-glucose DMEM supplemented with 10% FBS, 1 mM sodium pyruvate and 20 µg/ml gentamicin (all from Sigma) at 37 ºC in a humidified atmosphere with 5% CO_2.

To obtain SAR024 cell line (sporadic MPNST model), tissue samples from MPNST/024 patient were collected during sarcoma resection at Ghent University Hospital under sterile conditions. The patient did not receive any neo-adjuvant treatment. After tumor resection, tumor samples were immediately harvested under sterile conditions. A biopsy of 2 cm^3 tumor tissue was collected in 30 ml of DMEM supplemented with 10% FBS and antibiotics (100 µg/mL streptomycin, 100 U/mL penicillin). The sample was then immediately transferred to the laboratory for development of patient-derived cell lines. Cold ischaemia time for tumor samples was maximum 20min. Tumor tissue was cut into pieces of 1-2 mm^3. For development of a single cell suspension, 2-4 g was digested in 2,5 mL collagenase II solution (500 U/mL) and 2,5 mL DNase I solution (22KU/mL) and processed according to the gentleMACS Dissociator™ (Miltenyi Biotec) tumor digestion protocol. The remaining suspension was filtered through a 100 µm cell strainer (Corning) and the lysate was centrifuged at 1000 rpm for 5min. After removing the supernatant, the red pellet was resuspended in erythrocyte lysis buffer, to remove remnant red blood cells. The pellet was then resuspended in DMEM + 10% FBS + 100 U/mL penicillin and 100 µg/mL streptomycin (Life Technologies) to stop the reaction. The suspension was centrifuged again at 1000 rpm for 5min, resulting in a white pellet. The cells were resuspended and seeded into 6-well plates in DMEM + 10% FBS + 100 U/mL penicillin + 100 µg/mL streptomycin and incubated at 37°C in a 5% CO_2 humidified atmosphere.

All cell cultures were monthly tested for Mycoplasma by using MycoAlert Plus Kit (Lonza).

Gene silencing by lentiviral transduction

For shRNA-mediated knockdown of *ENG*, lentiviral particles encoding shRNA designed to silence human *ENG* (shENG) or a non-targeting control scrambled sequence (shScramble) were purchased from Santa Cruz Biotechnology. MPNST cells were transduced with the lentiviruses at a low MOI. After 48 hours, infected cells were selected by incubation with 1 µg/ml puromycin (Sigma).

Cell signaling assays

$2x10^5$ MPNST cells were seeded on 6-well plates. Upon 90% confluency, cells were serum-starved overnight in the presence of the anti-human ENG monoclonal antibody (mAb) TRC105 (TRACON Pharmaceuticals), the MEKi PD-0325901 (CNIO Experimental Therapeutics Unit, ETP), the combination of both drugs or IgG control (Jackson ImmunoResearch). TRC105 and IgG were resuspended in PBS and used at a final concentration of 50 µg/ml, and PD-0325901 was reconstituted in DMSO and used at a final concentration of 10 nM for STS26T cells or 1 nM for ST88-14 cells to analyze the synergy between the two compounds. Next day, cells were stimulated with 50 ng/ml recombinant human BMP-9 (R&D Systems) and 150 ng/ml recombinant

human VEGF (PeproTech) for one hour. Cells were lysed, protein content was determined, and Western blot analysis was performed (see below).

Animal studies

All mouse work was approved by the Institutional Ethics Committees of the CNIO (IACUC-006-2016), the Instituto de Salud Carlos III (CBA-15_2017) and the Comunidad Autónoma de Madrid (PROEX 168/17). 6-to 8-week-old female athymic nude and NOD scid gamma (NSG) mice were obtained from ENVIGO or CNIO Animal Facility, respectively.

To analyze the effect of *ENG* depletion in MPNST, nude mice were subcutaneously injected with $1x10^6$ shScramble- or shENG-STS26T cells (in a mix of 1:1 serum-free DMEM/Matrigel). Tumor growth was monitored twice weekly by caliper measurement of the two orthogonal large and small external diameters (a, b), and tumor volume was calculated by: a x b2 x π/6. When tumors reached 1.5 cm^3, mice were sacrificed, and tumors and lymph nodes (LN) were collected and processed for histology.

For anti-ENG and/or MEKi treatment of subcutaneous xenografts, $1x10^6$ STS26T or $3x10^6$ MPNST-SP-10 cells (in a mix of 1:1 serum-free DMEM/Matrigel) were injected subcutaneously into both flanks of athymic nude or NSG mice, respectively. When tumors reached ~100 mm^3 on average, mice were treated with the anti-ENG mAbs TRC105 and M1043 (TRACON Pharmaceuticals) or the MEKi PD-0325901 (CNIO-ETP), in monotherapy or combination regimens, as stated in Results. Control groups received thrice-weekly oral administrations of vehicle and/or biweekly intraperitoneal injections of IgG (Jackson Immunoresearch; 10mg/Kg diluted in PBS). TRC105 and M1043 were administrated intraperitoneally at 10 mg/Kg diluted in PBS twice weekly, a clinically relevant dose recommended by TRACON Pharmaceuticals for safety and efficacy issues. For PD-0325901, we selected 2 mg/Kg dissolved in 0.5% methylcellulose/0.2% Tween-80, oral gavage three times weekly as the most appropriate dosage to evaluate effects of its combination with anti-ENG therapies, based on pilot animal studies performed in collaboration with CNIO-ETP. For validation in additional MPNST models, $1x10^6$ SAR024 or $10x10^6$ ST88-14 cells (in a mix of 1:1 serum-free DMEM/Matrigel) were injected subcutaneously into both flanks of athymic nude or NSG mice, respectively. One week later, mice were treated with the anti-ENG therapies (TRC105/M1043) or IgG control as described above. Tumor volume was measured as previously indicated. At the end of treatment as mentioned in results section, mice were sacrificed and tumors were excised and processed for histology or RNA extraction. Sentinel LNs were also collected from athymic nude mice and analyzed for the presence of metastases by hematoxylin and eosin (H&E) staining.

For lung metastasis studies, $1x10^6$ luciferase-expressing STS26T cells were injected via tail vein in nude mice. One-week later, *in vivo* bioluminescence imaging (BLI) was performed using a Xenogen IVIS-200 machine (PerkinElmer), and mice were subsequently randomized into treatment groups (IgG plus vehicle, PD-0325901 alone, PD-0325901+TRC105/M1043) based on equal lung metastatic burden. Dose and treatment schedule were performed as described above. Metastasis was monitored twice weekly by *in vivo* BLI and, after three weeks of treatment, mice were sacrificed and lungs were imaged *ex vivo*.

RNA extraction, sequencing and data analysis

Total RNA from tissues or cells was extracted using the TRIZOL Reagent (Invitrogen). After recovery of the aqueous phase using chloroform, DNase treatment and further purification were performed using the RNeasy Mini Kit (Qiagen), following the manufacturer's instructions.

RNA sequencing (RNA-seq) was conducted by the CNIO Genomics Unit. Total RNA (1 µg) from samples was used. The average sample RNA Integrity Number was 9.65 (Agilent 2100 Bioanalyzer). cDNA libraries were generated using the Illumina TruSeq RNA Sample Preparation kit and sequenced on an Illumina HiSeq 2500 sequencer. Single-end 50-bp sequenced reads were analyzed with the nextpresso pipeline (18) as follows: sequencing quality was checked with FastQC v.0.10.1. Reads were aligned to the human genome (GRCh37/hg19) with TopHat-2.0.10 using Bowtie v.1.0.0 and SAMtools v.0.1.1.9, allowing two mismatches and 20 multihits. Differential expression was calculated with Cufflinks v.2.2.1 using the human GRCh37/hg19 transcript annotations from https://ccb.jhu.edu/software/tophat/igenomes.shtml. GSEA Preranked was used to perform GSEA of the described gene signatures on a pre-ranked gene list, setting 1,000 gene set permutations. For RNA-seq from MPNST xenografts, an initial filtering was done with Xenome to remove reads coming from mouse. Only those gene sets with FDR *q*-value < 0.25 were considered significant.

Quantitative real time PCR (qRT-PCR)

Total RNA (1 µg) was first reverse-transcribed using the QuantiTect Reverse Transcription kit (Qiagen). 20 ng of total cDNA were then subjected to qRT-PCR using TaqMan Gene Expression Master Mix and pre-designed TaqMan probes (all from Applied Biosystems, Supplementary Table 1). Assays were performed in triplicates on a 7500 Fast Real-Time PCR System (Applied Biosystems). Relative expression was calculated using the ΔΔCt method. *HPRT1* was used as housekeeping gene.

Immunoblotting

Cells were lysed in RIPA buffer supplemented with protease/phosphatase inhibitors (Roche). Protein concentration was determined by Pierce BCA assay (Thermo Fisher). Equal amounts of protein were resolved by SDS-PAGE and probed with the primary antibodies listed in Supplementary Table 2. Anti-rabbit and anti-mouse IgG-HRP-conjugated antibodies (GE Healthcare) were used as secondary antibodies. Signals were detected using the ECL Western Blotting Substrate kit (GE Healthcare). The intensities of immunoreactive bands were quantified by densitometry using ImageJ software (NIH).

Histological analyses

Tissue samples were fixed in 10% neutral buffered formalin (4% formaldehyde in solution) and embedded in paraffin, and 3-µm-thick sections were stained with H&E or processed for immunohistochemistry (IHC). Briefly, sections were deparaffinized and antigen retrieval was performed using Tris-EDTA (pH9). Endogenous peroxidase activity was quenched with 3%

hydrogen peroxide, and slides were then incubated with the appropriate primary antibodies (Supplementary table 2). An UltraVision ONE Detection System (Thermo Fisher) was used following the manufacturer's protocols. Sections were counterstained with hematoxylin (Anatech) and mounted with permanent mounting medium. Image analysis was performed using the ZEN software (Zeiss). ENG staining in human tumor tissues was scored by four independent pathologists according to the intensity and extent of expression (0-3).

Regarding ALU-II *in situ* hybridization, an automatic platform was used to run it (Ventana Discovery ULTRA, Roche). After deparaffinization and rehydration, antigen retrieval was first performed with the selected buffer (ULTRA CC2, 5424542001, Ventana, Roche) and Discovery Protease III (760-2020, Ventana, Roche). Slides were then incubated with the probe Alu positive control probe II (Ventana, Roche 05272041001) labeled with DNP. After the probe, samples were subjected to stringency washes three times and incubated with an intermediate, Rabbit anti-DNP (780-4335, Ventana, Roche). Visualization systems were needed (OmniMap anti-rabbit, Ventana, Roche) conjugated with horseradish peroxidase; immunohistochemical reaction was developed using DAB as a chromogen (ChromoMap DAB, Ventana, Roche) and nuclei were counterstained with Carazzi's hematoxylin.

For image analysis, whole slides were acquired with a slide scanner (AxioScan Z1, Zeiss). Five 2-mm^2 rectangular ROIs (Regions Of Interest) were randomly selected in the digital images of each tumor tissue sample for quantification. Different images from different slides were chosen for setting up the quantification program (AxioVision 4.6 software package, Zeiss) and an appropriate script for each antibody was created. Positivity was evaluated in one phase (phase 1, positive area) and compared with total tissue area (phase 2, total area). After script optimization, the quantification program was run and results were exported as excel files with scoring data for each tiff file. Data obtained were then compiled and appropriately assessed.

Statistical analysis

All analyses were performed using GraphPad Prism software v.9.1.0. Data are presented as mean ± SEM unless otherwise indicated. Specific number of independent experiments and biological replicates are stated in the figure legends. Differences between two groups were calculated using two-tailed unpaired Student's *t* test or Mann-Whitney test; for multiple groups, one-way ANOVA or Kruskal-Wallis (nonparametric) test were used. Tumor growth curves were analyzed by two-way ANOVA. *P*-values are indicated in each figure for statistically significant comparisons ($p<0.05$).

Data Availability

The authors confirm that the data supporting the findings of this study are available. Raw data generated in this study are available upon reasonable request from the corresponding author. RNA-seq data generated are publicly available in Gene Expression Omnibus (GEO) under the accession number **GSE216792** (RNA-seq after knockdown of *ENG* in STS26T cells compared to

shScramble control) and **GSE219148** (RNA-seq on the STS26T xenografts treated with TRC105/M1043 and compared their expression profiles with those of IgG-treated control tumors).

RESULTS

ENG is overexpressed in human primary and metastatic MPNSTs and plasma circulating sEVs.

Based on the data supporting a pro-tumorigenic role of ENG in sarcomas (16,17), we hypothesized that ENG could be also involved in PNST transformation, growth and/or metastasis. We first analyzed ENG expression by IHC in human benign PNs (n=39), pre-malignant lesions (ANNUBPs, n=9) and MPNSTs (n=38) collected from four independent patient cohorts. We found a higher expression of ENG in both tumor cells and ECs in MPNSTs compared to ANNUBPs or benign PNs (**Fig. 1A**, **B** and **Supplementary Fig. 1A**). Next, we examined ENG expression in a human TMA comprising primary and local recurrent MPNSTs and metastases. Analysis of ENG staining in both tumor cells and ECs showed that the expression of this protein increased in local recurrent tumors, being significantly higher in metastatic lesions compared to primary tumors (**Fig. 1C**, **D** and **Supplementary Fig. 1B**).

We evaluated the relevance of circulating ENG in PNST by analyzing the levels of both soluble and EV-shed ENG in the plasma of 44 patients with PNSTs at different stages (benign PNs and MPNSTs) and 23 healthy controls. We separated plasma soluble proteins from sEVs using standard ultracentrifugation methods. sEV number and protein concentration did not differ based on tumor stage (**Supplementary Fig. 1C,D**). Analysis of ENG protein concentration by ELISA showed no significant differences in the expression of soluble ENG between the groups (**Fig. 1E**). However, the levels of ENG in sEVs were significantly increased in MPNST patients compared to patients bearing benign PNs or healthy controls (**Fig. 1F**).

ENG contributes to the acquisition of malignant traits in MPNST cells

To explore the functional importance of ENG in MPNSTs, we first analyzed its expression in a panel of established human MPNST cell lines. High ENG protein levels were observed in all these cell lines, except for the S462 model (**Fig. 2A**). We then silenced *ENG* expression in STS26T and ST88-14 cells by lentiviral-mediated delivery of shRNAs. STS26T cell line derives from a sporadic MPNST (19) and ST88-14 is a NF1-associated cell line with confirmed loss of heterozygosity at the *NF1* locus (20). We verified that ENG mRNA and protein levels were reduced by 80% in *ENG*-depleted STS26T and ST88-14 cells (shENG) compared to their respective controls (shScramble) (**Fig. 2B**,**C**).

To examine the gene expression changes related to *ENG* silencing in MPNST cells, we performed RNA-seq after knockdown of *ENG* in STS26T cells compared to shScramble control. *ENG* depletion caused notable changes in the transcriptome of STS26T cells, leading to a significant

deregulation of 951 genes (FDR<0.05) (**Supplementary Fig. 2A** and **Supplementary Table 3**). Gene Set Enrichment Analysis (GSEA) revealed a significant suppression of gene signatures associated with oncogenic traits, including soluble angiogenic factors (e.g. VEGFA, PDGF, PLGF) and metastasis (**Fig. 2D** and **Supplementary Fig. 2B,C**). Accordingly, the downregulation of several pro-angiogenic factors (e.g. *VEGF*, *PDGFc*, *FGF*) and pro-metastatic genes (e.g. *THBS*, *POSTN*, *SEMA5*, *ITGB1*, *S100A1*) upon *ENG* depletion was confirmed at the mRNA level in both STS26T and ST88-14 cells (**Fig. 2E**,**F**).

We next analyzed signaling pathways affected by ENG in MPNST cells. This TGF-β coreceptor is known to modulate TGF-β signaling by promoting the ALK1-Smad1/5 pathway (15). Moreover, ENG can mediate non-canonical, non-Smad pathways such as the MAPK/ERK signaling cascade (21), which plays crucial roles in MPNST malignancy and progression (8). We thus focused on evaluating the importance of ENG for these signaling pathways in MPNST cells. *ENG* silencing significantly reduced the phosphorylation of Smad1/5 and ERK1/2 in both the sporadic cell line STS26T and the NF1-derived cell line ST88-14 (**Fig. 2G**,**H**).

ENG promotes MPNST growth and metastasis *in vivo*

We next studied the effect of *ENG* depletion on MPNST *in vivo.* STS26T-shENG- or –shScramble cells were subcutaneously implanted into nude mice. Downregulation of *ENG* significantly reduced xenograft growth (**Fig. 3A**). Moreover, we analyzed spontaneous metastasis at end-point (day 32 post-tumor cell injection) by H&E staining (**Supplementary Fig. 3A**) and we found that the number and size of LN metastases were decreased in mice bearing *ENG*-depleted xenografts compared to those with control tumors (**Fig. 3B**). Western blot and IHC studies confirmed a strong reduction of ENG protein levels in xenografts arising from shENG cells (**Supplementary Fig. 3B,C**). In order to dissect the mechanisms underlying the role of ENG in MPNST *in vivo*, we analyzed the effect of *ENG* knockdown on both tumor cell proliferation and death. We did not find differences in the expression of the apoptotic marker active caspase-3 between shScramble and shENG tumors (**Supplementary Fig. 3D,E**). However, we observed that *ENG* knockdown significantly reduced tumor cell proliferation as denoted by the strong decrease in the number of $Ki67^+$ cells (**Fig. 3C**,**D**). Moreover, *ENG* depletion in tumor cells significantly reduced tumor vascularization in STS26T xenografts, as determined by staining for the EC marker CD31 (**Fig. 3E**,**F**).

Pharmacological targeting of ENG decreases MPNST growth and metastasis

We next ascertained whether ENG could be exploited as potential therapeutic target in MPNSTs. Based on our data showing that ENG is upregulated in tumor cells and also in the vasculature of human MPNSTs, we tested a therapeutic strategy to block ENG on both tumor cells and ECs in MPNST xenografts using a combination of the anti-human and anti-mouse ENG mAbs TRC105 and M1043, respectively (12).

Notably, administration of TRC105/M1043 to nude mice bearing established STS26T xenografts (~100 mm^3 average) resulted in a significant decrease in both primary tumor growth and LN metastatic burden (**Fig. 4A**,**B** and **Supplementary Fig. 4A**). To confirm the efficacy of anti-ENG therapy in an additional MPNST model, we used early-passage patient-derived MPNST-SP-10 cells subcutaneously injected into NSG mice. Co-treatment with TRC105/M1043 after tumor establishment (~100 mm^3 average) significantly reduced tumor growth also in this MPNST xenograft model (**Fig. 4C**). We also validated the anti-tumor efficacy of anti-ENG treatment in SAR024 and ST88-14 models (**Supplementary Fig. 4B-F,** materials and methods). We confirmed the human origin of ST88-14 cells and development in xenografts of murine supportive stroma by performing *in situ* hybridization with Alu probes specific to human cells (**Supplementary Fig. 4G,** materials and methods). Together, these data revealed that ENG-blocking antibodies decrease MPNST growth and metastasis, suggesting that anti-ENG therapies could represent a novel treatment option for this tumor type.

To analyze the genes and molecular pathways modulated by ENG targeting, we performed RNA-seq on the STS26T xenografts treated with TRC105/M1043 and compared their expression profiles with those of IgG-treated control tumors. Consistent with our *in vitro* results, several pro-angiogenic and pro-metastatic human genes were significantly downregulated in these tumors upon ENG inhibition (**Fig. 4D**). Accordingly, we found a significant suppression of gene signatures related to angiogenesis and metastasis (**Fig. 4E,F**). We validated a subset of pro-angiogenic (e.g. *VEGFR1*, *NFATC4*, *PLXDC1*) and pro-metastatic (e.g. *SEMA5*, *POSTN*, *ITGA1*, *THBS2*) genes by qRT-PCR (**Fig. 4G**). Likewise, using IHC analysis, we demonstrated that VEGF expression was significantly reduced in ST88-14 xenografts as a consequence of ENG targeting (**Supplementary Fig. 4H**). Moreover, immunohistochemical staining of CD31 confirmed a significant reduction of tumor vascularization in STS26T (see below in Fig. 6C,E), MPNST-SP-10 (**Fig. 4H,I**) and ST88-14 (**Supplementary Fig. 4I**) xenografts treated with TRC105/M1043. In line with our data using the *ENG* knockdown model, pharmacological targeting of ENG also significantly reduced tumor cell proliferation in STS26T (see below in Fig. 6C,D) and ST88-14 tumors (**Supplementary Fig. 4J**), as denoted by the decrease in the number of $Ki67^+$ cells.

Combination therapy with anti-ENG antibodies and the MEKi PD-0325901 efficiently inhibits MPNST growth and metastasis

MEK inhibition is a promising strategy for the treatment of PNSTs, which commonly harbor hyperactivation of the MAPK/ERK signaling pathway (8). Indeed, MEKis have become the first FDA-approved therapy for patients with PNs, recognized precursors of MPNSTs, and they have demonstrated strong albeit variable efficacy in preclinical MPNST models, leading to ongoing clinical trials (e.g. NCT03433183; NCT05253131, (6,22)). We thus set out to evaluate the use of the combination of anti-ENG mAbs with a MEKi.

We first tested the efficacy of this combination treatment in already established primary MPNSTs. STS26T and MPNST-SP-10 cell lines were subcutaneously injected into athymic nude or NSG mice, respectively, and tumors were allowed to develop (~100 mm^3 average). Mice were then treated with the anti-ENG antibodies TRC105/M1043 alone, the MEKi PD-0325901 alone, the combination of PD-0325901 with TRC105/M1043 (combo) or IgG plus vehicle (control). Tumor growth was monitored (**Fig. 5A**). Consistent with previously reported data (8), PD-0325901 reduced significantly yet variably tumor growth in STS26T and MPNST-SP-10 xenograft models (**Fig. 5B,C**). Notably, PD-0325901 plus TRC105/M1043 synergistically reduced the growth of STS26T tumors (**Fig. 5B** and **Supplementary Fig. 5A**). In MPNST-SP-10 xenografts, which were more sensitive to PD-0325901 alone, the combination treatment significantly decreased tumor growth compared to control and anti-ENG group, and it led to more pronounced, albeit not statistically significant, anti-tumor effects than MEKi monotherapy (**Fig. 5C**). Analysis of spontaneous metastasis in STS26T xenografts at end-point showed that both anti-ENG and MEKi monotherapies reduced the total number of LN metastatic foci but only the combination therapy led to a statistically significant decrease in LN metastasis (**Fig. 5D,E**). No adverse effects of drug treatment on body weight or skin were observed (**Supplementary Fig. 5B**).

Given that up of 50% of MPNST patients develop metastatic disease, normally to the lung (23), we next analyzed the impact of the combination therapy on distant metastasis. Nude mice were injected via tail vein with luciferase-expressing STS26T cells, which exhibit metastatic tropism to the lung (24). One week later, mice with established metastases were distributed into the control and treated groups (PD-0325901 alone, PD-0325901+TRC105/M1043) based on equal bioluminescent signal (**Supplementary 5C**), and metastatic growth was followed by *In vivo* Imaging System (IVIS, **Fig. 5F**). Although PD-0325901 monotherapy reduced lung metastasis, only the combination treatment with TRC105/M1043 demonstrated a statistically significant decrease in MPNST metastatic outgrowth and lung metastatic burden at end-point (**Fig. 5G-J** and **Supplementary Fig. 5D,E**).

ENG targeting and MEK inhibition cooperatively reduce Smad1/5 and MAPK/ERK pathway activation, MPNST cell proliferation and angiogenesis

To explore the molecular mechanisms modulated by the anti-ENG and MEKi combination therapy in MPNSTs, we analyzed its effect on ENG-Smad1/5 and MAPK/ERK pathway activation in tumor cells. STS26T and ST88-14 cells were treated with TRC105 alone, PD-0325901 alone, the combination of both or IgG control and subsequently stimulated with BMP-9, the main ENG ligand (25), and VEGF, an important activator of the MAPK/ERK pathway (26). We found that only the TRC105/PD-0325901 combination significantly reduced ENG expression and Smad1/5 phosphorylation in both STS26T and ST88-14 cells (**Fig. 6A,B** and **Supplementary Fig. 6A,B**). Although MEKi treatment increased p-MEK1/2 levels consistent with signaling rebound upon feedback relief (27), it led to diminished phosphorylation of ERK, the direct downstream target of MEK (**Fig. 6A,B** and **Supplementary Fig. 6A,B**). TRC105 alone also produced a significant

decrease in p-ERK levels (**Fig. 6A,B** and **Supplementary Fig. 6A,B**). Importantly, dual targeting of ENG and MEK resulted in synergistic inhibition of ERK1/2 phosphorylation in the two MPNST cell lines (**Fig. 6A,B** and **Supplementary Fig. 6A,B**). These data indicate that ENG targeting cooperates with MEK inhibition to block the activation of both ENG-Smad1/5 and MAPK/ERK pathways in MPNST cells.

Given the role of these pathways in cancer cell proliferation and angiogenesis (26) together with our data demonstrating that ENG promotes MPNST cell proliferation and vascularization, we next analyzed the effect of dual blockade of ENG and MEK on these biological processes in MPNSTs. IHC analysis of Ki67 showed that both ENG targeting with TRC105/M1043 and MEK inhibition with PD-0325901 significantly reduced tumor cell proliferation in STS26T xenografts (**Fig. 6C,D**). Notably, the combination treatment was significantly more effective than either anti-ENG or MEKi monotherapy in inhibiting tumor cell proliferation in these tumors (**Fig. 6C,D**). In addition, as indicated above, TRC105/M1043 anti-ENG treatment decreased the number of $CD31^+$ vessels in STS26T tumors (**Fig. 6C,E**). These anti-angiogenic effects were significantly enhanced upon combination with PD-0325901 (**Fig. 6C,E**).

DISCUSSION

The highly aggressive and metastatic behavior of MPNSTs (23) and the absence of effective systemic treatments (5,8) underscore the urgent need to identify novel mediators of pathogenesis that are amenable to therapeutic intervention. In this study, we show that the TGF-β coreceptor ENG is a novel player and a promising therapeutic target in MPNSTs.

ENG expression has been reported in different human sarcomas, correlating with malignancy, aggressiveness or worse survival (28-32). Here we demonstrate that ENG is highly expressed on both tumor cells and ECs in human MPNSTs and that its expression correlates with advanced stages of the disease (local recurrence and distant metastasis), providing evidence for the use of both tumor and endothelial ENG as markers of MPNST transformation. Unfortunately, tissue biopsy presents limitations for the management of MPNST patients, mainly due to tumor location and intratumoral heterogeneity (23). Liquid biopsy, which is emerging as a non-invasive method for early cancer detection (33), remains poorly explored in MPNSTs. The use of circulating biomarkers such as circulating-free DNA (cfDNA) (34) or sEVs (this study) may represent an attractive non-invasive approach for early MPNST detection and monitoring, an idea that must be further developed in the field. We found that ENG levels were increased in plasma-circulating sEVs from patients with MPNSTs compared to PN patients or healthy controls. Besides ENG abundance in tumor tissue, high levels of two circulating forms of ENG (soluble and in association with EVs) have been detected in plasma from patients with breast, prostate and colorectal cancer, correlating with disease progression (35-38). To date, only one study has investigated the potential of EV-shed ENG as a circulating biomarker in cancer patients, showing that plasma concentration of ENG^+ EVs significantly distinguished breast cancer patients from healthy

subjects (38). Our data suggest that EV-secreted ENG could be a potential liquid biopsy biomarker to detect malignant transformation of PNSTs. Nevertheless, it is important to note that these results have to be interpreted with caution, since ENG overexpression was observed only in some MPNST patients, which could be attributed to the heterogeneity of human disease. Unfortunately, in our series we did not have access to matched tumor and plasma samples or follow-up information. Studies with larger paired tissue/blood specimens, in particular during follow-up and linked clinical data, would be crucial to validate ENG's potential utility in liquid biopsies.

ENG mainly modulates malignant phenotypes of cancer cells by regulating TGF-β/BMP/Smad signaling but also Smad-independent pathways such as the MAPK/ERK signaling cascade (16), which plays crucial roles in MPNST tumor growth (8). Consistent with other studies in different tumor models (32,39), we found that *ENG* downregulation attenuated Smad1/5 pathway activation in both the sporadic cell line STS26T and the NF1-associated cell line ST88-14. Likewise, *ENG* knockdown led to reduced ERK1/2 phosphorylation in these MPNST cells, which is in agreement with a prior report revealing that *ENG* depletion in uterine leiomyosarcoma cells decreased p-ERK1/2 levels, impairing cell invasion (29). However, it was shown that ENG expression in transformed epidermal cells inhibited the MAPK/ERK pathway, thus suppressing H-RAS-mediated oncogenic transformation (40). Therefore, the precise function of ENG in regulating MAPK/ERK signaling seems to depend on tumor cell type, sarcoma versus carcinoma, which appears to be associated with pro-tumoral or anti-tumoral effects, respectively. Our data, together with previous results proposing that a crosstalk between Smad1/5 and MAPK/ERK signaling pathways promotes MPNST cell aggressiveness (41), suggest a role for ENG in favoring the communication between these pathways, thus potentially contributing to malignant behavior of MPNST cells.

Indeed, we demonstrate that ENG expression in MPNST cells favors tumor growth and metastasis *in vivo*, as *ENG* knockdown resulted in reduced tumor cell proliferation and impaired tumor growth and metastasis. Accordingly, previous studies showed that *ENG* depletion decreased the metastatic abilities of different sarcoma cell lines (28,29,32,42) and inhibited *in vivo* progression of Ewing sarcoma cells (32), indicating a pro-tumoral action of ENG in sarcoma cells. However, the role of ENG in carcinoma cells is context-dependent, in some cases (e.g. melanoma, pancreatic, renal and ovarian cancer) promoting tumor progression and aggressiveness, whereas in other cases (e.g. spindle cell carcinoma, esophageal, lung and breast cancer) it has been associated with tumor suppression (16). These findings point to specific effects of ENG on tumorigenesis depending on the type/origin of tumor cells (mesenchymal versus epithelial), which could be associated with differences in ENG expression levels and modulation of Smad and non-Smad pathways. Interestingly, although endothelial ENG has been widely reported to promote vascularization in different cancer mouse models (12,43-45), our study shows that ENG expression in tumor cells indirectly stimulates angiogenesis within the TME. Together, our data support a dual role for tumor cell-specific ENG in MPNST affecting both tumor

cells and the TME. In tumor cells, ENG appears to favor Smad1/5 and MAPK/ERK pathway activation and metastatic gene expression, promoting cell proliferation and metastatic behavior. Moreover, ENG can stimulate angiogenesis within the TME via induction of soluble pro-angiogenic factors. Thus, both tumor cell-autonomous and non-autonomous mechanisms mediate ENG contribution to MPNST growth and metastasis.

Notably, this study demonstrates that ENG may be a promising therapeutic target for MPNSTs, since targeting tumor and endothelial ENG with TRC105/M1043 inhibited tumor growth and metastasis in MPNST xenograft models. Pharmacological ENG inhibition resulted in reduced *in vivo* proliferation and metastatic ability of MPNST cells and impaired tumor angiogenesis, which is consistent with our data from the *ENG* knockdown model and, therefore, supports the involvement of ENG in these biological processes in MPNSTs. Since, in addition to tumor cells and ECs, ENG expression has been reported in other cell types within the TME (e.g. fibroblasts) (46), we cannot rule out the possibility that the therapeutic effects of anti-ENG therapy in our MPNST xenografts are also due to ENG inhibition in these stromal cells. In line with our findings, several studies revealed that anti-ENG mAbs efficiently suppress tumor growth and metastasis in different mouse tumor models (12). Indeed, in phase I-III trials, TRC105, alone or in combination therapy, has shown a favorable safety profile and promising efficacy in patients with diverse tumor types, mainly in those with some advanced STS subtypes (12-14). Here, our preclinical data support a novel use of TRC105 for the treatment of MPNSTs.

MEK inhibition is emerging as a promising therapeutic approach for the treatment of PNSTs, which commonly harbor hyperactivation of the MAPK/ERK signaling pathway (8). In fact, MEKis represent the most effective targeted therapy for patients with PNs, which may evolve to MPNSTs (22). In MPNST, only a single clinical case report has shown durable efficacy of MEKi monotherapy to date (47); however, extensive *in vivo* evidence indicates robust yet variable and transient anti-tumor effects of MEK inhibition alone (6), denoting a limited activity of MEKis as single agent in MPNST. Therefore, based on the current data, MEKis may be more effective in combination with other agents (8). Our data demonstrate that the combination of the anti-ENG mAbs TRC105/M1043 with PD-0325901 efficiently inhibits tumor growth in MPNST xenograft models. We found that the combination treatment significantly improved the therapeutic efficacy of MEKi monotherapy in STS26T xenografts, and it led to more pronounced, albeit not statistically significant, anti-tumor effects compared to MEK inhibition alone in MPNST-SP-10 tumors, which were more sensitive to PD-0325901. Importantly, analysis of MPNST-SP-10 model showed that this tumor is 100% $Ki67^+$ (data not shown), suggesting that the combined effect of anti-ENG/MEK inhibition could be affected by baseline proliferation and sensitivity to single-agent MEKi. Further studies are needed to correlate basal response to MEK inhibition alone with the effect of MEKi plus anti-ENG. These analyses will facilitate the selection of patients who could benefit from this combination therapy.

Mechanistically, we found that ENG targeting cooperated with MEK inhibition to block ENG-Smad1/5 and MAPK/ERK pathway activation in MPNST cells and to reduce tumor cell

proliferation and angiogenesis in STS26T primary tumors. These data suggest that a (direct and/or indirect) cross-talk between ENG-Smad1/5 and MAPK/ERK pathways can contribute to tumor growth in this model, presumably through effects on: i) tumor cells (promotion of proliferation) and ii) the TME (stimulation of angiogenesis). Therefore, it is plausible that the improved anti-tumor efficacy of the anti-ENG and anti-MEK combination therapy can be a consequence of cooperative inhibition of these pathways.

The inhibitory effects of the dual therapy on both primary tumor growth and established metastases suggest that the treatment could be effective for localized or metastatic disease. These findings have important translational implications, since intervention timing and disease staging have been reported as possible causes of failure of clinical trials involving MPNST patients (23). Importantly, several phase I-II studies have demonstrated the feasibility, safety and preliminary efficacy of combining anti-angiogenic agents (e.g. sorafenib or pazopanib) with a MEKi in patients with different solid malignancies, mainly in patients with other STS subtypes (8). TRC105 is emerging as a more promising strategy than these classic anti-angiogenic drugs for the treatment of cancer patients (16). Indeed, the clinical effects of TRC105 have been attributed to the inhibition of angiogenesis (48) but also to the targeting of tumor cells and immunosuppressive cells (e.g. T and B regulatory cells), which has been associated with reduced metastasis and better survival (49-51). These multi-target effects of TRC105 contribute to its favorable efficacy in cancer patients (12). These data, together with our *in vivo* results, provide support for clinical investigation of TRC105 alone or in combination with a MEKi as a novel therapeutic strategy for MPNSTs.

In summary, our findings unveil a tumor-promoting function of ENG in MPNSTs and support the use of this protein as a novel biomarker and a promising therapeutic target for this disease. We also provide evidence that dual targeting of ENG and MEK may represent an attractive treatment option for MPNSTs, particularly for those with modest sensitivity to single-agent MEKi.

Acknowledgments:

We apologize to those authors whose work could not be cited due to size limitations. We thank Dr. Eduard Serra, Dr. Conxi Lázaro and Dr. David Lyden for their support in the project. We also thank Héctor Tejero for his help in analyzing RNA-seq data. Dr. Peinado laboratory is funded by US Department of Defense (W81XWH-16-1-0131), Agencia Estatal de Investigación/Ministerio de Ciencia e Innovación (AEI/MCIN) (PID2020-118558RB-I00/AEI/10.13039/501100011033), Fundación Proyecto Neurofibromatosis, European Union's Horizon 2020 research and innovation programme "proEVLifeCycle" under the Marie Skłodowska-Curie grant agreement No 860303, and Fundación Científica AECC. We are also grateful for the support of the Ministerio de Universidades (Programa de Formación de Profesorado Universitario (FPU)) for the fellowship FPU016/05356 awarded to T. González-Muñoz and to the Translational NeTwork for the CLinical application of Extracellular VesicleS (TeNTaCLES) RED2018-102411-T(AEI/10.13039/501100011033). A. Di Giannatale was supported during this work by a research grant from Nuovo-Soldati Foundation. The CNIO, certified as Severo Ochoa Excellence Centre, is supported by the Spanish Government through the Instituto de Salud Carlos III.

REFERENCES

1. Farid M, Demicco EG, Garcia R, Ahn L, Merola PR, Cioffi A*, et al.* Malignant peripheral nerve sheath tumors. *Oncologist* 2014;**19**(2):193-201 doi 10.1634/theoncologist.2013-0328.
2. Korfhage J, Lombard DB. Malignant Peripheral Nerve Sheath Tumors: From Epigenome to Bedside. *Mol Cancer Res* 2019;**17**(7):1417-28 doi 10.1158/1541-7786.MCR-19-0147.
3. Gutmann DH, Ferner RE, Listernick RH, Korf BR, Wolters PL, Johnson KJ. Neurofibromatosis type 1. *Nat Rev Dis Primers* 2017;**3**:17004 doi 10.1038/nrdp.2017.4.
4. Prudner BC, Ball T, Rathore R, Hirbe AC. Diagnosis and management of malignant peripheral nerve sheath tumors: Current practice and future perspectives. *Neurooncol Adv* 2020;**2**(Suppl 1):i40-i9 doi 10.1093/noajnl/vdz047.
5. Bradford D, Kim A. Current treatment options for malignant peripheral nerve sheath tumors. *Curr Treat Options Oncol* 2015;**16**(3):328 doi 10.1007/s11864-015-0328-6.
6. Martin E, Lamba N, Flucke UE, Verhoef C, Coert JH, Versleijen-Jonkers YMH*, et al.* Non-cytotoxic systemic treatment in malignant peripheral nerve sheath tumors (MPNST): A systematic review from bench to bedside. *Crit Rev Oncol Hematol* 2019;**138**:223-32 doi 10.1016/j.critrevonc.2019.04.007.
7. Mohamad T, Plante C, Brosseau JP. Toward Understanding the Mechanisms of Malignant Peripheral Nerve Sheath Tumor Development. *Int J Mol Sci* 2021;**22**(16) doi 10.3390/ijms22168620.
8. Gonzalez-Munoz T, Kim A, Ratner N, Peinado H. The need for new treatments targeting MPNST: the potential of strategies combining MEK inhibitors with antiangiogenic agents. *Clin Cancer Res* 2022 doi 10.1158/1078-0432.CCR-21-3760.
9. Gesundheit B, Parkin P, Greenberg M, Baruchel S, Senger C, Kapelushnik J*, et al.* The role of angiogenesis in the transformation of plexiform neurofibroma into malignant peripheral nerve sheath tumors in children with neurofibromatosis type 1. *J Pediatr Hematol Oncol* 2010;**32**(7):548-53 doi 10.1097/MPH.0b013e3181e887c7.
10. Wasa J, Nishida Y, Suzuki Y, Tsukushi S, Shido Y, Hosono K*, et al.* Differential expression of angiogenic factors in peripheral nerve sheath tumors. *Clin Exp Metastasis* 2008;**25**(7):819-25 doi 10.1007/s10585-008-9197-8.
11. Nishida Y, Urakawa H, Nakayama R, Kobayashi E, Ozaki T, Ae K*, et al.* Phase II clinical trial of pazopanib for patients with unresectable or metastatic malignant peripheral nerve sheath tumors. *Int J Cancer* 2021;**148**(1):140-9 doi 10.1002/ijc.33201.
12. Liu Y, Paauwe M, Nixon AB, Hawinkels L. Endoglin Targeting: Lessons Learned and Questions That Remain. *Int J Mol Sci* 2020;**22**(1) doi 10.3390/ijms22010147.
13. Attia S, Sankhala KK, Riedel RF, Robinson SI, Conry RM, Boland PM*, et al.* A phase 1B/ phase 2A study of TRC105 (Endoglin Antibody) in combination with pazopanib (P) in patients (pts) with advanced soft tissue sarcoma (STS). *Journal of Clinical Oncology* 2016;**34**(15_suppl):11016- doi 10.1200/JCO.2016.34.15_suppl.11016.
14. Mehta CR, Liu L, Theuer C. An adaptive population enrichment phase III trial of TRC105 and pazopanib versus pazopanib alone in patients with advanced angiosarcoma (TAPPAS trial). *Ann Oncol* 2019;**30**(1):103-8 doi 10.1093/annonc/mdy464.
15. Lebrin F, Goumans MJ, Jonker L, Carvalho RL, Valdimarsdottir G, Thorikay M*, et al.* Endoglin promotes endothelial cell proliferation and TGF-beta/ALK1 signal transduction. *EMBO J* 2004;**23**(20):4018-28 doi 10.1038/sj.emboj.7600386.
16. Gonzalez Munoz T, Amaral AT, Puerto-Camacho P, Peinado H, de Alava E. Endoglin in the Spotlight to Treat Cancer. *Int J Mol Sci* 2021;**22**(6) doi 10.3390/ijms22063186.
17. Rosen LS, Gordon MS, Robert F, Matei DE. Endoglin for targeted cancer treatment. *Curr Oncol Rep* 2014;**16**(2):365 doi 10.1007/s11912-013-0365-x.

18. Graña O, Rubio-Camarillo M, Fdez-Riverola F, Pisano DG, Glez-Peña D. Nextpresso: Next Generation Sequencing Expression Analysis Pipeline. *Current Bioinformatics* 2018;**13**(6):583-91 doi http://dx.doi.org/10.2174/1574893612666170810153850.
19. Dahlberg WK, Little JB, Fletcher JA, Suit HD, Okunieff P. Radiosensitivity in vitro of human soft tissue sarcoma cell lines and skin fibroblasts derived from the same patients. *Int J Radiat Biol* 1993;**63**(2):191-8 doi 10.1080/09553009314550251.
20. Glover TW, Stein CK, Legius E, Andersen LB, Brereton A, Johnson S. Molecular and cytogenetic analysis of tumors in von Recklinghausen neurofibromatosis. *Genes Chromosomes Cancer* 1991;**3**(1):62-70 doi 10.1002/gcc.2870030111.
21. Lee NY, Blobe GC. The interaction of endoglin with beta-arrestin2 regulates transforming growth factor-beta-mediated ERK activation and migration in endothelial cells. *J Biol Chem* 2007;**282**(29):21507-17 doi 10.1074/jbc.M700176200.
22. Casey D, Demko S, Sinha A, Mishra-Kalyani PS, Shen YL, Khasar S*, et al.* FDA Approval Summary: Selumetinib for Plexiform Neurofibroma. *Clin Cancer Res* 2021;**27**(15):4142-6 doi 10.1158/1078-0432.CCR-20-5032.
23. Kim A, Stewart DR, Reilly KM, Viskochil D, Miettinen MM, Widemann BC. Malignant Peripheral Nerve Sheath Tumors State of the Science: Leveraging Clinical and Biological Insights into Effective Therapies. *Sarcoma* 2017;**2017**:7429697 doi 10.1155/2017/7429697.
24. Ghadimi MP, Young ED, Belousov R, Zhang Y, Lopez G, Lusby K*, et al.* Survivin is a viable target for the treatment of malignant peripheral nerve sheath tumors. *Clin Cancer Res* 2012;**18**(9):2545-57 doi 10.1158/1078-0432.CCR-11-2592.
25. Nolan-Stevaux O, Zhong W, Culp S, Shaffer K, Hoover J, Wickramasinghe D*, et al.* Endoglin requirement for BMP9 signaling in endothelial cells reveals new mechanism of action for selective anti-endoglin antibodies. *PLoS One* 2012;**7**(12):e50920 doi 10.1371/journal.pone.0050920.
26. Dhillon AS, Hagan S, Rath O, Kolch W. MAP kinase signalling pathways in cancer. *Oncogene* 2007;**26**(22):3279-90 doi 10.1038/sj.onc.1210421.
27. Wang J, Pollard K, Allen AN, Tomar T, Pijnenburg D, Yao Z*, et al.* Combined Inhibition of SHP2 and MEK Is Effective in Models of NF1-Deficient Malignant Peripheral Nerve Sheath Tumors. *Cancer Res* 2020;**80**(23):5367-79 doi 10.1158/0008-5472.CAN-20-1365.
28. Sakamoto R, Kajihara I, Miyauchi H, Maeda-Otsuka S, Yamada-Kanazawa S, Sawamura S*, et al.* Inhibition of Endoglin Exerts Antitumor Effects through the Regulation of Non-Smad TGF-beta Signaling in Angiosarcoma. *J Invest Dermatol* 2020;**140**(10):2060-72 e6 doi 10.1016/j.jid.2020.01.031.
29. Mitsui H, Shibata K, Mano Y, Suzuki S, Umezu T, Mizuno M*, et al.* The expression and characterization of endoglin in uterine leiomyosarcoma. *Clin Exp Metastasis* 2013;**30**(6):731-40 doi 10.1007/s10585-013-9574-9.
30. Boeuf S, Bovee JV, Lehner B, van den Akker B, van Ruler M, Cleton-Jansen AM*, et al.* BMP and TGFbeta pathways in human central chondrosarcoma: enhanced endoglin and Smad 1 signaling in high grade tumors. *BMC Cancer* 2012;**12**:488 doi 10.1186/1471-2407-12-488.
31. Gromova P, Rubin BP, Thys A, Cullus P, Erneux C, Vanderwinden JM. ENDOGLIN/CD105 is expressed in KIT positive cells in the gut and in gastrointestinal stromal tumours. *J Cell Mol Med* 2012;**16**(2):306-17 doi 10.1111/j.1582-4934.2011.01315.x.
32. Pardali E, van der Schaft DW, Wiercinska E, Gorter A, Hogendoorn PC, Griffioen AW*, et al.* Critical role of endoglin in tumor cell plasticity of Ewing sarcoma and melanoma. *Oncogene* 2011;**30**(3):334-45 doi 10.1038/onc.2010.418.
33. Cescon DW, Bratman SV, Chan SM, Siu LL. Circulating tumor DNA and liquid biopsy in oncology. *Nat Cancer* 2020;**1**(3):276-90 doi 10.1038/s43018-020-0043-5.
34. Szymanski JJ, Sundby RT, Jones PA, Srihari D, Earland N, Harris PK*, et al.* Cell-free DNA ultra-low-pass whole genome sequencing to distinguish malignant peripheral nerve

sheath tumor (MPNST) from its benign precursor lesion: A cross-sectional study. *PLoS Med* 2021;**18**(8):e1003734 doi 10.1371/journal.pmed.1003734.

35. Li C, Guo B, Wilson PB, Stewart A, Byrne G, Bundred N*, et al.* Plasma levels of soluble CD105 correlate with metastasis in patients with breast cancer. *Int J Cancer* 2000;**89**(2):122-6 doi 10.1002/(sici)1097-0215(20000320)89:2<122::aid-ijc4>3.0.co;2-m.
36. Svatek RS, Karam JA, Roehrborn CG, Karakiewicz PI, Slawin KM, Shariat SF. Preoperative plasma endoglin levels predict biochemical progression after radical prostatectomy. *Clin Cancer Res* 2008;**14**(11):3362-6 doi 10.1158/1078-0432.CCR-07-4707.
37. Nogues A, Gallardo-Vara E, Zafra MP, Mate P, Marijuan JL, Alonso A*, et al.* Endoglin (CD105) and VEGF as potential angiogenic and dissemination markers for colorectal cancer. *World J Surg Oncol* 2020;**18**(1):99 doi 10.1186/s12957-020-01871-2.
38. Douglas SR, Yeung KT, Yang J, Blair SL, Cohen O, Eliceiri BP. Identification of CD105+ Extracellular Vesicles as a Candidate Biomarker for Metastatic Breast Cancer. *J Surg Res* 2021;**268**:168-73 doi 10.1016/j.jss.2021.06.050.
39. Bernabeu C, Lopez-Novoa JM, Quintanilla M. The emerging role of TGF-beta superfamily coreceptors in cancer. *Biochim Biophys Acta* 2009;**1792**(10):954-73 doi 10.1016/j.bbadis.2009.07.003.
40. Santibanez JF, Perez-Gomez E, Fernandez LA, Garrido-Martin EM, Carnero A, Malumbres M*, et al.* The TGF-beta co-receptor endoglin modulates the expression and transforming potential of H-Ras. *Carcinogenesis* 2010;**31**(12):2145-54 doi 10.1093/carcin/bgq199.
41. Ahsan S, Ge Y, Tainsky MA. Combinatorial therapeutic targeting of BMP2 and MEK-ERK pathways in NF1-associated malignant peripheral nerve sheath tumors. *Oncotarget* 2016;**7**(35):57171-85 doi 10.18632/oncotarget.11036.
42. Postiglione L, Di Domenico G, Caraglia M, Marra M, Giuberti G, Del Vecchio L*, et al.* Differential expression and cytoplasm/membrane distribution of endoglin (CD105) in human tumour cell lines: Implications in the modulation of cell proliferation. *Int J Oncol* 2005;**26**(5):1193-201 doi 10.3892/ijo.26.5.1193.
43. Paauwe M, Heijkants RC, Oudt CH, van Pelt GW, Cui C, Theuer CP*, et al.* Endoglin targeting inhibits tumor angiogenesis and metastatic spread in breast cancer. *Oncogene* 2016;**35**(31):4069-79 doi 10.1038/onc.2015.509.
44. Romero D, O'Neill C, Terzic A, Contois L, Young K, Conley BA*, et al.* Endoglin regulates cancer-stromal cell interactions in prostate tumors. *Cancer Res* 2011;**71**(10):3482-93 doi 10.1158/0008-5472.CAN-10-2665.
45. Duwel A, Eleno N, Jerkic M, Arevalo M, Bolanos JP, Bernabeu C*, et al.* Reduced tumor growth and angiogenesis in endoglin-haploinsufficient mice. *Tumour Biol* 2007;**28**(1):1-8 doi 10.1159/000097040.
46. Paauwe M, Schoonderwoerd MJA, Helderman R, Harryvan TJ, Groenewoud A, van Pelt GW*, et al.* Endoglin Expression on Cancer-Associated Fibroblasts Regulates Invasion and Stimulates Colorectal Cancer Metastasis. *Clin Cancer Res* 2018;**24**(24):6331-44 doi 10.1158/1078-0432.CCR-18-0329.
47. Nagabushan S, Lau LMS, Barahona P, Wong M, Sherstyuk A, Marshall GM*, et al.* Efficacy of MEK inhibition in a recurrent malignant peripheral nerve sheath tumor. *NPJ Precis Oncol* 2021;**5**(1):9 doi 10.1038/s41698-021-00145-8.
48. Liu Y, Starr MD, Brady JC, Dellinger A, Pang H, Adams B*, et al.* Modulation of circulating protein biomarkers following TRC105 (anti-endoglin antibody) treatment in patients with advanced cancer. *Cancer Med* 2014;**3**(3):580-91 doi 10.1002/cam4.207.
49. Rosen LS, Hurwitz HI, Wong MK, Goldman J, Mendelson DS, Figg WD*, et al.* A phase I first-in-human study of TRC105 (Anti-Endoglin Antibody) in patients with advanced cancer. *Clin Cancer Res* 2012;**18**(17):4820-9 doi 10.1158/1078-0432.CCR-12-0098.

50. Apolo AB, Karzai FH, Trepel JB, Alarcon S, Lee S, Lee MJ*, et al.* A Phase II Clinical Trial of TRC105 (Anti-Endoglin Antibody) in Adults With Advanced/Metastatic Urothelial Carcinoma. *Clin Genitourin Cancer* 2017;**15**(1):77-85 doi 10.1016/j.clgc.2016.05.010.
51. Karzai FH, Apolo AB, Cao L, Madan RA, Adelberg DE, Parnes H*, et al.* A phase I study of TRC105 anti-endoglin (CD105) antibody in metastatic castration-resistant prostate cancer. *BJU Int* 2015;**116**(4):546-55 doi 10.1111/bju.12986.

Figure legends

Figure 1. ENG is upregulated in human MPNST tissues and plasma circulating sEVs. A) Immunohistochemical staining for ENG in the indicated PNSTs. Scale bar=50μm, and **B)** their distribution (%) according to ENG expression. Score 0-1, low ENG staining; 2, intermediate ENG staining and 3, high ENG staining. PNs n=39, ANNUBPs n=9, and MPNSTs n=38 from four independent patient cohorts. * P<0.05, **** P<0.0001 by Kruskal-Wallis test. **C)** Representative images of ENG IHC staining in a human TMA comprising locally recurrent MPNSTs and metastases. Scale bar=100μm. **D)** Quantification of ENG expression (score 0-3). Primary tumors (MPNST (P)) n=10, local recurrent tumors n=6 and metastases n=2. * P<0.05 by Kruskal-Wallis test. **E,F)** Quantification of ENG levels in EV-depleted soluble fraction (**E**) and circulating sEVs (**F**) collected from the plasma of healthy controls (n=23) and patients with benign (PNs, n=33) or malignant (MPNSTs, n=11) PNSTs. sEV-secreted ENG levels were normalized to the total amount of sEV protein. Mean ± s.e.m.; ns, not significant; * P<0.05 by one-way ANOVA.

Figure 2. ENG regulates oncogenic pathways in MPNST cells. **A)** Immunoblotting showing ENG protein levels in a panel of human MPNST cell lines. **B)** qRT-PCR analysis of *ENG* expression after shRNA-knockdown of *ENG* in the STS26T and ST88-14 cell lines. **C)** Western blot analysis of ENG in STS26T and ST88-14 cells transduced with lentiviral vectors coding for scramble- or ENG-shRNA. **D)** GSEA plots for the indicated gene signatures associated with pro-angiogenic factor VEGF-A and metastasis. **E**,**F)** qRT-PCR validation of the indicated angiogenic and metastatic genes in STS26T (**E**) and ST88-14 (**F**) cells upon *ENG* knockdown. **G,H)** Representative Western blot images (**G**) and quantification (**H**) of Smad1/5 and ERK1/2 phosphorylation in shScramble and shENG- STS26T and ST88-14 cells. p-Smad1/5 and p-ERK1/2 levels were normalized to total Smad1 and ERK1/2 levels, respectively. Data in **B,E,F,H** are presented as the fold change compared to shScramble. Mean ± s.e.m. of at least three biological replicates; * P<0.05, ** P<0.01, *** P<0.001, **** P<0.0001 by unpaired t-test.

Figure 3. *ENG* shRNA in tumor cells reduces MPNST growth and metastasis. A) Analysis of primary tumor growth in shScramble- and shENG-STS26T cells subcutaneously injected into both flanks of athymic nude mice. n=10 mice per group from two independent experiments. Mean ± s.e.m.; **** P<0.0001 by two-way ANOVA. **B)** LN metastatic burden was determined by H&E staining in LN sections at day 32 post-tumor cell injection (end-point). The black points encircle a representative metastasis. Scale bar=100μm. Quantification of the total number of metastatic foci

in the LNs (right panel). Lesions were binned into four size categories according to the number of tumor cells: single (1-2 cells), small (3-10 cells), micro (11-30 cells) and macro (greater than 30 cells). n=10 LNs per group; * P<0.05 by Mann-Whitney test. **C,D)** IHC analysis of Ki67 in shScramble- and shENG-STS26T xenografts (Scale bar=100μm) (**C**) and quantification (**D**). **E)** Representative images of CD31 immunohistochemical staining in the indicated tumors. Scale bar=100μm. **F)** Quantification of the number of $CD31^+$ vessels. Dots in the graphs in **D**,**F** represent the mean number of positive cells/vessels per field of each tumor (5 fields/tumor). Mean ± s.e.m.; ** P<0.01, *** P<0.001 by unpaired t-test.

Figure 4. Anti-ENG therapy decreases tumor growth in MPNST xenograft models. A) Growth curves of STS26T xenografts treated with TRC105 and M1043 (anti-ENG) or IgG control (10 mg/Kg twice a week). n=5 mice per group (10 tumors/treatment). **B)** H&E staining of representative LNs collected from mice bearing STS26T xenografts at the end of the treatment (day 28; upper panels). Metastases are highlighted by a discontinuous black line. Scale bar=100μm. Quantification of the total number of metastatic foci (lower panel). Lesions were divided into micro-metastasis (11-30 cells) and macro-metastasis (greater than 30 cells). n=10 LNs per group; * P<0.05 by Mann-Whitney test. **C)** Tumor growth of MPNST-SP-10 xenografts treated with TRC105/M1043 or IgG control (10 mg/Kg twice a week). n=4 mice per group (8 tumors/treatment). Arrow in **A,C** indicates the time point of start of treatment; data are presented as mean ± s.e.m.; *** P<0.001, **** P< 0.0001 by two-way ANOVA. **D)** Heat-map showing the significantly downregulated human genes in anti-ENG (TRC105/M1043)-treated STS26T xenografts compared to control IgG-treated tumors. n=3 tumors per group. FDR q-value<0.05. **E,F)** GSEA plots for the indicated gene sets related to angiogenesis (**E**) and metastasis (**F**) available in Molecular Signatures Database (MSigDB; anti-ENG versus IgG). **G)** qRT-PCR validation of the indicated genes obtained from RNA-seq results. Data were normalized to IgG. Mean ± s.e.m. of three biological replicates; * P< 0.05, ** P< 0.01 by unpaired t-test. **H,I)** IHC analysis of CD31 in MPNST-SP-10 xenografts collected at the completion of treatment (Scale bar=100μm) (**H**) and quantification (**I**). Dots in the graph represent the mean number of positive vessels per field of each tumor (5 fields/tumor). Mean ± s.e.m.; ** P<0.01 by unpaired t-test.

Figure 5. Combination treatment with anti-ENG and anti-MEK therapies inhibits MPNST growth and metastasis. A) Schematic of the experiment performed to analyze the effect of the anti-ENG/anti-MEK combination therapy in MPNST subcutaneous xenograft models. Dosages of each treatment are indicated with color sticks. **B,C)** Tumor growth of STS26T (**B**) and MPNST-SP-10 (**C**) xenografts treated with IgG plus vehicle (control), TRC105/M1043 (anti-ENG) alone, PD-0325901 (PD-901) alone or the combination of PD-901 and TRC105/M1043 (combo). n=5 mice per group (10 tumors/condition). Arrows indicate the time point of start of treatment. Mean ± s.e.m.; ns, not significant; ** P<0.01, *** P<0.001, **** P<0.0001 by two-way ANOVA. **D)** Analysis of LN metastases by H&E staining in STS26T xenografts at end-point (day 28). Metastases are highlighted by a discontinuous black line. Scale bar=100μm. **E)** Quantification of

the total number of metastatic foci. Lesions were divided into micro-metastasis (11-30 cells) and macro-metastasis (greater than 30 cells). n=10 LNs/group; ns, not significant; * P<0.05 by Mann-Whitney test. **F)** Schematic of the experiment performed to evaluate the effect of the anti-ENG/anti-MEK combination therapy on experimental MPNST lung metastasis. Dosages of each treatment are indicated with color sticks. **G,H)** Representative BLI images (**G**) and quantification (**H**) of experimental metastasis assay follow-up in mice receiving the indicated treatments. Data were normalized to the total flux mean from each group at day 7 (start of treatment). The arrow indicates the time point of start of treatment. **I)** Assessment of lung metastatic burden by *ex vivo* BLI at end-point (day 28), with **J)** quantification of total photon flux per lung lobe. n=4 mice per group. Data are mean ± s.e.m.; ns, not significant; * P<0.05 by two-way ANOVA in (**H**) and ** P< 0.01 by one-way ANOVA in (**J**).

Figure 6. Dual inhibition of ENG and MEK cooperates to reduce Smad1/5 and MAPK/ERK signaling activity, tumor cell proliferation and angiogenesis. A, B) Representative Western blot images (**A**) and quantification (**B**) of ENG expression and Smad1/5, MEK and ERK activation in STS26T cells pre-treated overnight with a IgG control, the anti-human ENG mAb TRC105 alone, the MEKi PD-0325901 (PD-901) alone or the combination of both drugs (combo) and then stimulated with BMP-9/VEGF for 1 hour. Cells without neither the pre-treatment nor BMP-9/VEGF stimulation were used as a control. Phosphorylated protein levels were normalized to the corresponding total protein levels. Data are presented as the fold change compared to IgG. Mean ± s.e.m. of four biological replicates; * P<0.05, ** P<0.01, **** P<0.0001 by one-way ANOVA. **C)** IHC of Ki67 and CD31 in STS26T xenografts from mice treated with IgG plus vehicle (control), the anti-ENG mAbs TRC105 and M1043 (anti-ENG), PD-901 alone or the combination of TRC105/M1043 with PD-901 (combo). **D, E)** Quantification of the number of $Ki67^+$ cells (**D**) and $CD31^+$ vessels (**E**) in tumor sections (5 fields/tumor). Dots in the graphs represent the mean number of positive stained cells/vessels per field of each tumor. Mean ± s.e.m.; * P<0.05, *** P<0.001 by one-way ANOVA.

Supplementary figure 1. Analysis of ENG expression and plasma circulating sEVs in human PNSTs. A) Representative images of ENG immunohistochemical staining in the indicated PNSTs. Scale bar= 100µm. **B)** IHC analysis of ENG in a human TMA comprising locally recurrent MPNSTs and metastases. Scale bar= 100µm. **C,D)** Quantification of total number of particles per milliliter using Nanoparticle Tracking Analysis (Nanosight) (**C**) and protein concentration in circulating sEVs (**D**) from the plasma of healthy controls (n=23) and patients with benign (PNs, n=33) or malignant (MPNSTs, n=11) PNSTs. Mean ± s.e.m.; ns, not significant by one-way ANOVA.

Supplementary figure 2. *ENG* knockdown leads to downregulation of pro-angiogenic and pro-metastatic gene signatures in MPNST cells. **A)** Heat-map representation of the differentially expressed genes in shENG- versus shScramble-STS26T cells (FDR q-value<0.05).

B,C) GSEA plots for the indicated gene signatures associated with pro-angiogenic factors (**B**) and metastasis (**C**) in shENG STS26T cells compared to shScramble cells. Signatures were obtained from Molecular Signatures Database (MSigDB).

Supplementary figure 3. *ENG* knockdown does not affect MPNST cell apoptosis *in vivo*. A) H&E-stained LN sections showing representative examples of macrometastasis (more than 30 cells), micrometastasis (11-30 cells) and small metastasis (3-10 cells). Arrows indicate single human metastatic cells that were quantified by a pathologist. Please advise that human tumor cell nuclei are bigger than mouse LN cells. Scale bar=100µm. **B)** Western blot analysis of ENG in shScramble- and shENG-STS26T xenografts. **C)** Representative images of ENG immunohistochemical staining in STS26T xenografts at end-point (day 32). Scale bar=200µm. **D,E)** IHC analysis of the apoptotic marker active-caspase 3 in the indicated STS26T xenografts (Scale bar=100µm) (**D**) and quantification (**E**). Dots in the graph represent the mean number of positive cells per field of each tumor (5 fields/tumor). Mean ± s.e.m.; ns, not significant by unpaired t-test.

Supplementary figure 4. Anti-ENG therapy is active against MPNST xenografts. A) Representative images of mice bearing STS26T xenografts treated with IgG or TRC105/M1043 at end-point (day 28). Scale bar=1cm. n= 5 mice per group. **B)** Tumor growth of SAR024 xenografts treated with TRC105/M1043 (anti-ENG) or IgG control (10 mg/Kg twice a week). n=4 mice per group (8 tumors/condition). **C)** Waterfall plot showing change in tumor volume (represented as log2 fold change) of individual SAR024 tumors formed at 28 days after transplant and after 21 days with pharmacological inhibition. ** P<0.01 by unpaired t-test. **D)** ST88-14 xenograft growth in mice treated with TRC105/M1043 or IgG control (10 mg/Kg twice a week). n= 5 mice per group (10 tumors/treatment). Arrow in **B,D** indicates the time point of start of treatment; data are presented as mean ± s.e.m.; *** P<0.001, **** P< 0.0001 by two-way ANOVA. **E)** Representative bioluminescence images (upper panels) and total flux quantification (lower panel) in control- and TRC105/M1043-treated ST88-14 tumors at end-point (day 28). Data correspond to mean ± s.e.m. of 10 tumors per condition; * P<0.05 by unpaired t-test. **F)** Waterfall plot representing change in tumor volume (log2 fold change) of individual tumors at 28 days after transplant and 21 days after pharmacological inhibition. *** P<0.001 by unpaired t-test. **G)** Representative images of *in situ* hybridization of the indicated xenografts with Alu probes specific to human cells. Scale bar=100µm. Inserts show higher magnification images of the area outlined in black (Scale bar=25µm). **H-J)** IHC analysis of VEGF (**H**), CD31 (**I**) and Ki67 (**J**) in IgG- and anti-ENG-treated ST88-14 xenografts. Representative images from each group are shown in left panels. Scale bar of 25µm in **H** and 100µm in **I**,**J**. Dots in the graphs (right panels) represent the mean positive VEGF area/total area and the mean number of positive CD31-vessels and Ki67-cells per field of each tumor (5 fields/tumor). Mean ± s.e.m.; ** P<0.01, **** P<0.0001 by unpaired t-test.

Supplementary figure 5. Combined anti-ENG/anti-MEK therapy inhibits MPNST growth without toxicity *in vivo*. A) Plots showing growth of individual subcutaneous STS26T tumors in mice treated with IgG plus vehicle (control), TRC105/M1043 (anti-ENG) alone, PD-0325901 (PD-901) alone or the combination of PD-901 with TRC105/M1043 (combo). **B)** Percentage of body weight changes relative to day 0 along the treatment period. **C)** Randomization in the lung metastasis experiment based on lung bioluminescent signal before start of treatment (day 7 post-tumor cell injection). **D)** Changes in lung metastatic burden quantified by luciferin photon flux at 21 days after the indicated treatments. Data are presented as log2 fold change of total flux at end-point (day 28) compared to start of treatment (day 7). Mean ± s.e.m. of four mice per group; * P<0.05 by one-way ANOVA. **E)** Percentage of lung lobules with metastasis (bioluminiscent signal above background) in each group of treatment.

Supplementary figure 6. Dual inhibition of ENG and MEK efficiently blocks ENG-Smad1/5 and MAPK/ERK pathway activation in ST88-14 cells. A,B) Western blot analysis (**A**) and quantification (**B**) of ENG expression and Smad1/5, MEK and ERK phosphorylation in ST88-14 cells stimulated with BMP-9/VEGF in the presence of IgG control, the anti-human ENG mAb TRC105, the MEKi PD-0325901 (PD-901) or the combination of both drugs (combo). Cells without neither the treatment nor BMP-9/VEGF stimulation were used as a control. Phosphorylated protein levels were normalized to the corresponding total protein levels. Data are presented as the fold change compared to IgG. Mean ± s.e.m. of at least four biological replicates; * P<0.05, ** P<0.01, *** P<0.001, **** P<0.0001 by one-way ANOVA.

ABBREVIATIONS

ANNUBP	Atypical neurofibromatous neoplasms of uncertain biological potential
BCA	Bicinchoninic acid
BLI	Bioluminescence imaging
CBR	Clinical benefit rate
cfDNA	Circulating-free DNA
EC	Endothelial cell
ENG	Endoglin
ETP	Experimental Therapeutics Unit
GAP	GTPase activating protein
GSEA	Gene set enrichment analysis
H&E	Hematoxylin and eosin
IHC	Immunohistochemistry
LN	Lymph node
MEKi	MEK inhibitor
MPNST	Malignant peripheral nerve sheath tumor
NF1	Neurofibromatosis type 1
NSG	NOD scid gamma
NTA	Nanoparticle tracking analysis
PD-901	PD-0325901
PN	Plexiform neurofibroma
PNST	Peripheral nerve sheath tumor
RNA-seq	RNA sequencing
sEV	Small extracellular vesicle
STS	Soft-tissue sarcoma
TMA	Tissue microarray
TME	Tumor microenvironment

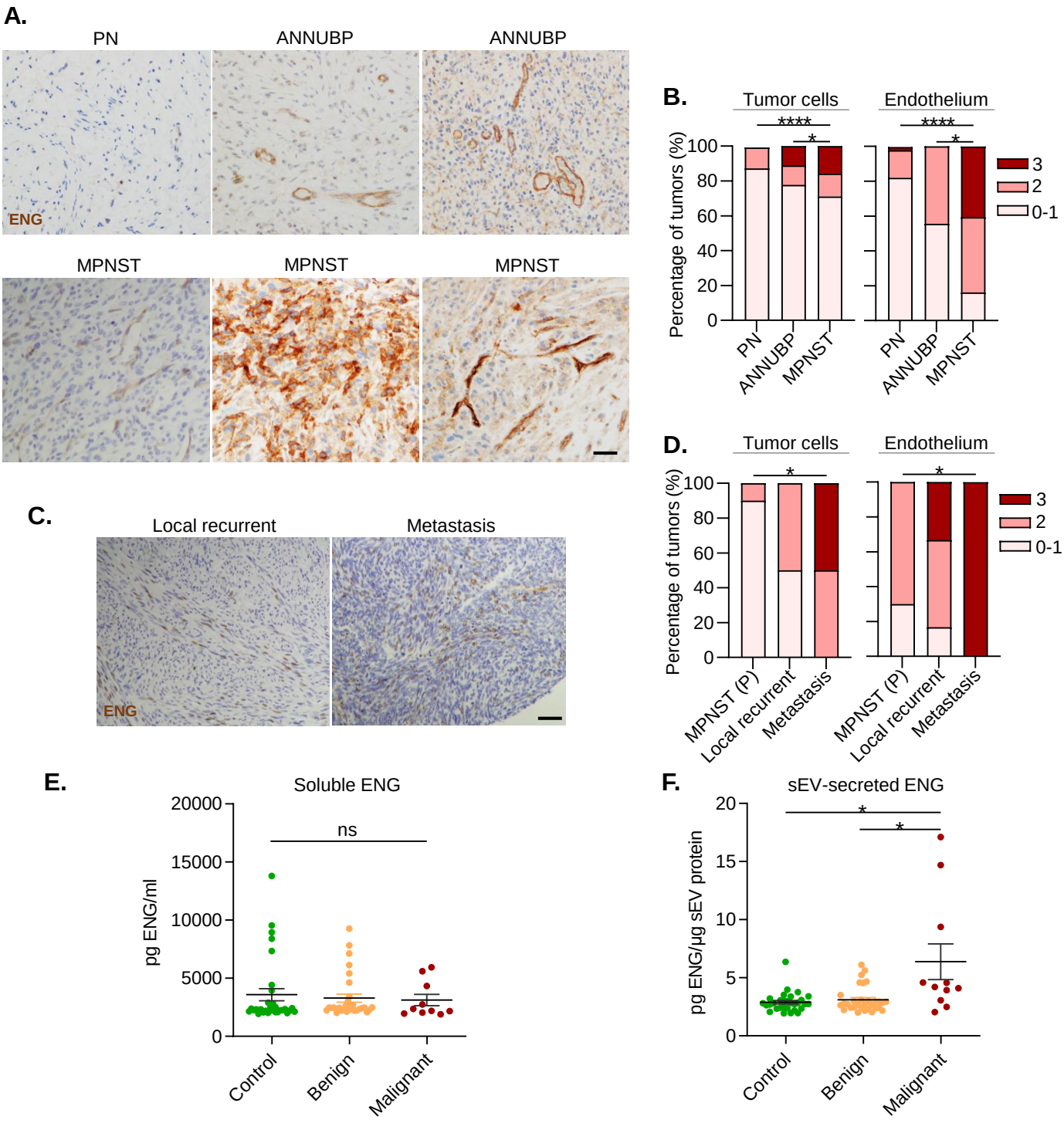
A.
PN
ANNUBP
ANNUBP
ENG
MPNST
MPNST
MPNST
B.
Tumor cells
Endothelium
****
*
****
*
Percentage of tumors (%)
100
80
60
40
20
0
PN
ANNUBP
MPNST
PN
ANNUBP
MPNST
3
2
0-1
C.
Local recurrent
Metastasis
ENG
D.
Tumor cells
Endothelium
*
*
Percentage of tumors (%)
100
80
60
40
20
0
MPNST (P)
Local recurrent
Metastasis
MPNST (P)
Local recurrent
Metastasis
3
2
0-1
E.
Soluble ENG
ns
pg ENG/ml
20000
15000
10000
5000
0
Control
Benign
Malignant
F.
sEV-secreted ENG
*
*
pg ENG/µg sEV protein
20
15
10
5
0
Control
Benign
Malignant

Figure 1

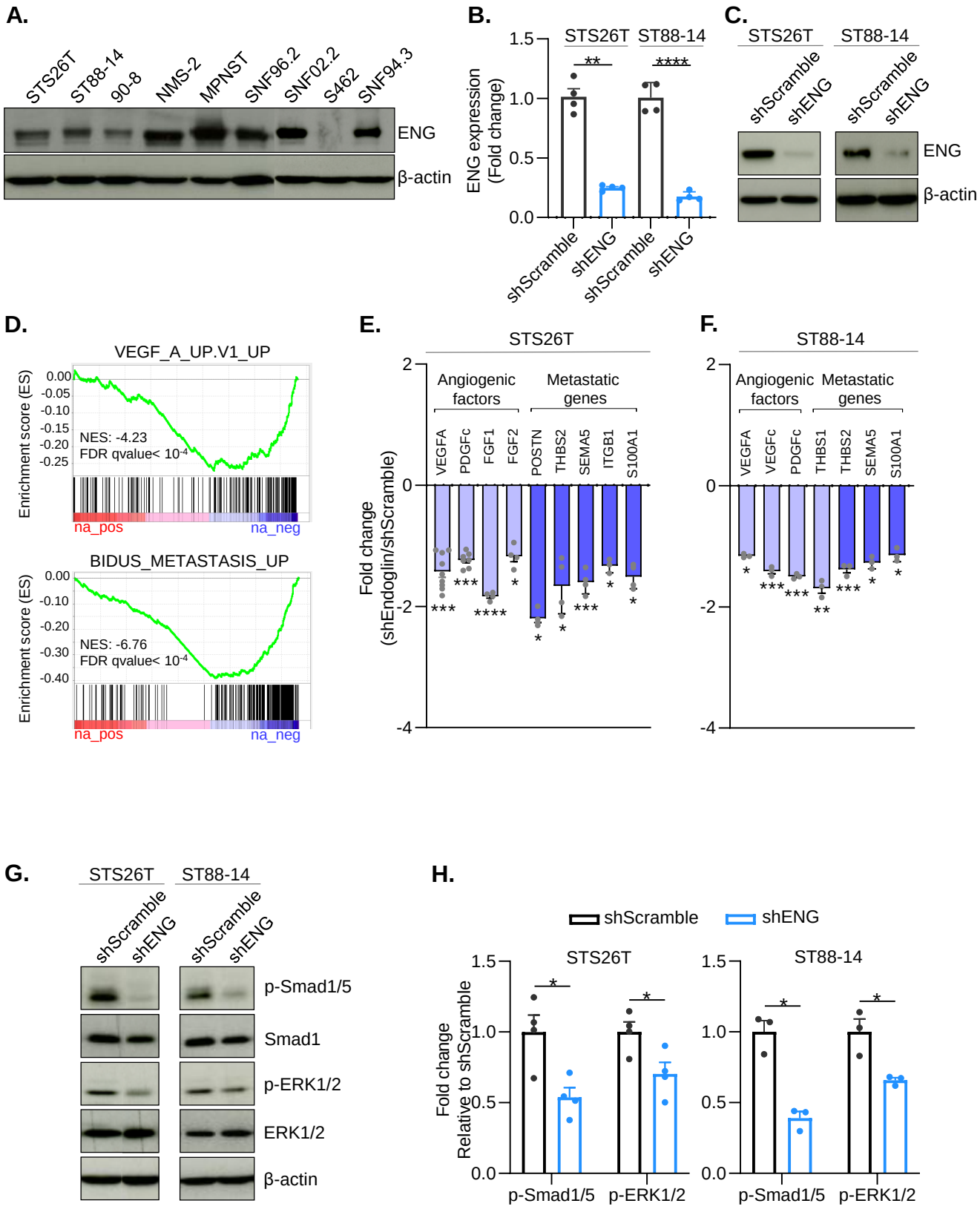
A.
STS26T
ST88-14
90-8
NMS-2
MPNST
SNF96.2
SNF02.2
S462
SNF94.3
ENG
β-actin
B.
STS26T
ST88-14
ENG expression (Fold change)
1.5
1.0
0.5
0.0
**
****
shScramble
shENG
shScramble
shENG
C.
STS26T
ST88-14
shScramble
shENG
shScramble
shENG
ENG
β-actin
D.
VEGF_A_UP.V1_UP
Enrichment score (ES)
0.00
-0.05
-0.10
-0.15
-0.20
-0.25
NES: -4.23
FDR qvalue< 10-4
na_pos
na_neg
BIDUS_METASTASIS_UP
Enrichment score (ES)
0.00
-0.10
-0.20
-0.30
-0.40
NES: -6.76
FDR qvalue< 10-4
na_pos
na_neg
E.
STS26T
Angiogenic factors
Metastatic genes
VEGFA
PDGFc
FGF1
FGF2
POSTN
THBS2
SEMA5
ITGB1
S100A1
Fold change (shEndoglin/shScramble)
2
0
-2
-4
F.
ST88-14
Angiogenic factors
Metastatic genes
VEGFA
VEGFc
PDGFc
THBS1
THBS2
SEMA5
S100A1
2
0
-2
-4
G.
STS26T
ST88-14
shScramble
shENG
shScramble
shENG
p-Smad1/5
Smad1
p-ERK1/2
ERK1/2
β-actin
H.
shScramble
shENG
STS26T
ST88-14
Fold change Relative to shScramble
1.5
1.0
0.5
0.0
p-Smad1/5
p-ERK1/2
p-Smad1/5
p-ERK1/2

Figure 2

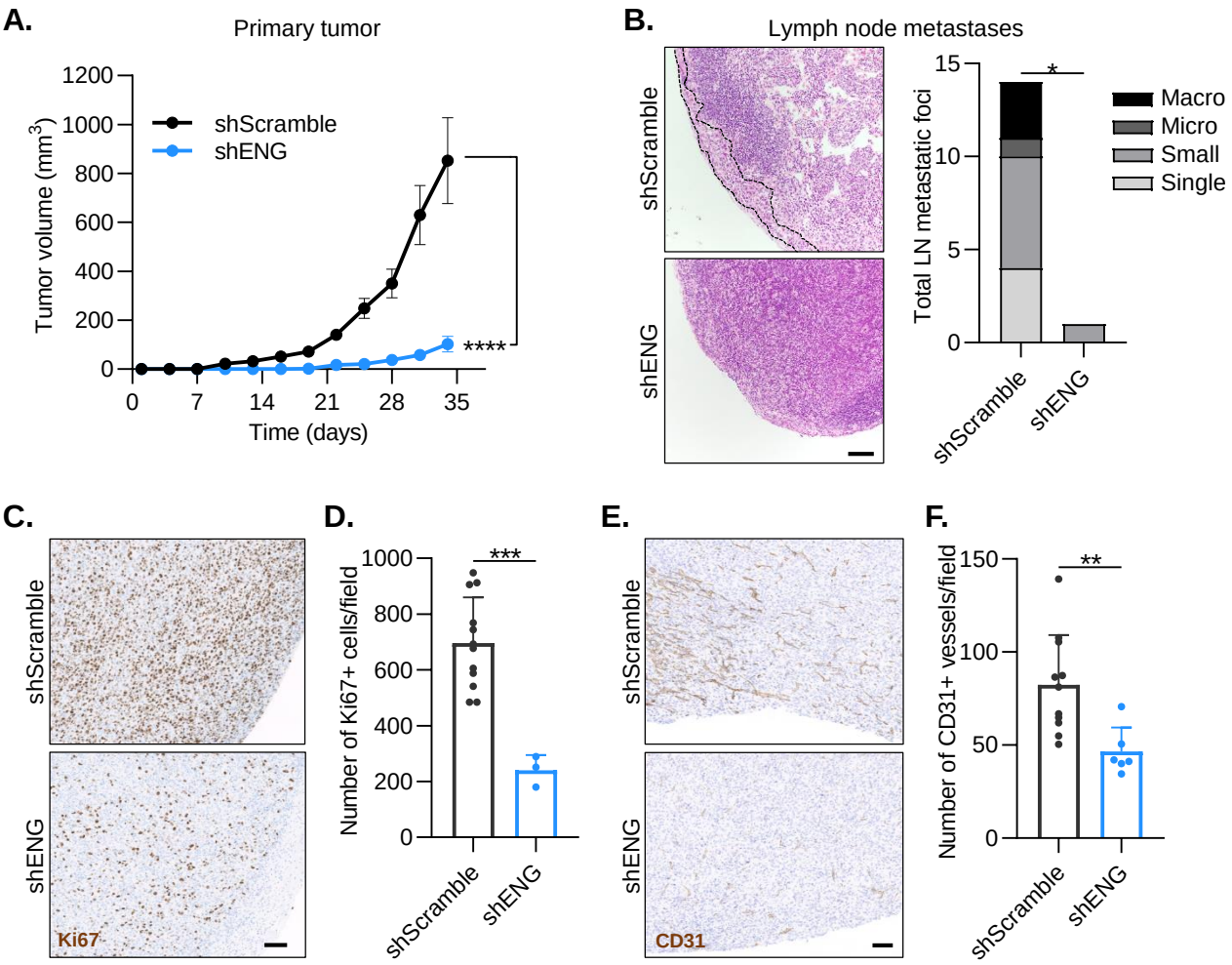
A.
Primary tumor
Tumor volume (mm3)
1200
1000
800
600
400
200
0
shScramble
shENG
****
0
7
14
21
28
35
Time (days)
B.
Lymph node metastases
shScramble
shENG
Total LN metastatic foci
15
10
5
0
*
Macro
Micro
Small
Single
shScramble
shENG
C.
shScramble
shENG
Ki67
D.
Number of Ki67+ cells/field
1000
800
600
400
200
0
***
shScramble
shENG
E.
shScramble
shENG
CD31
F.
Number of CD31+ vessels/field
150
100
50
0
**
shScramble
shENG

Figure 3

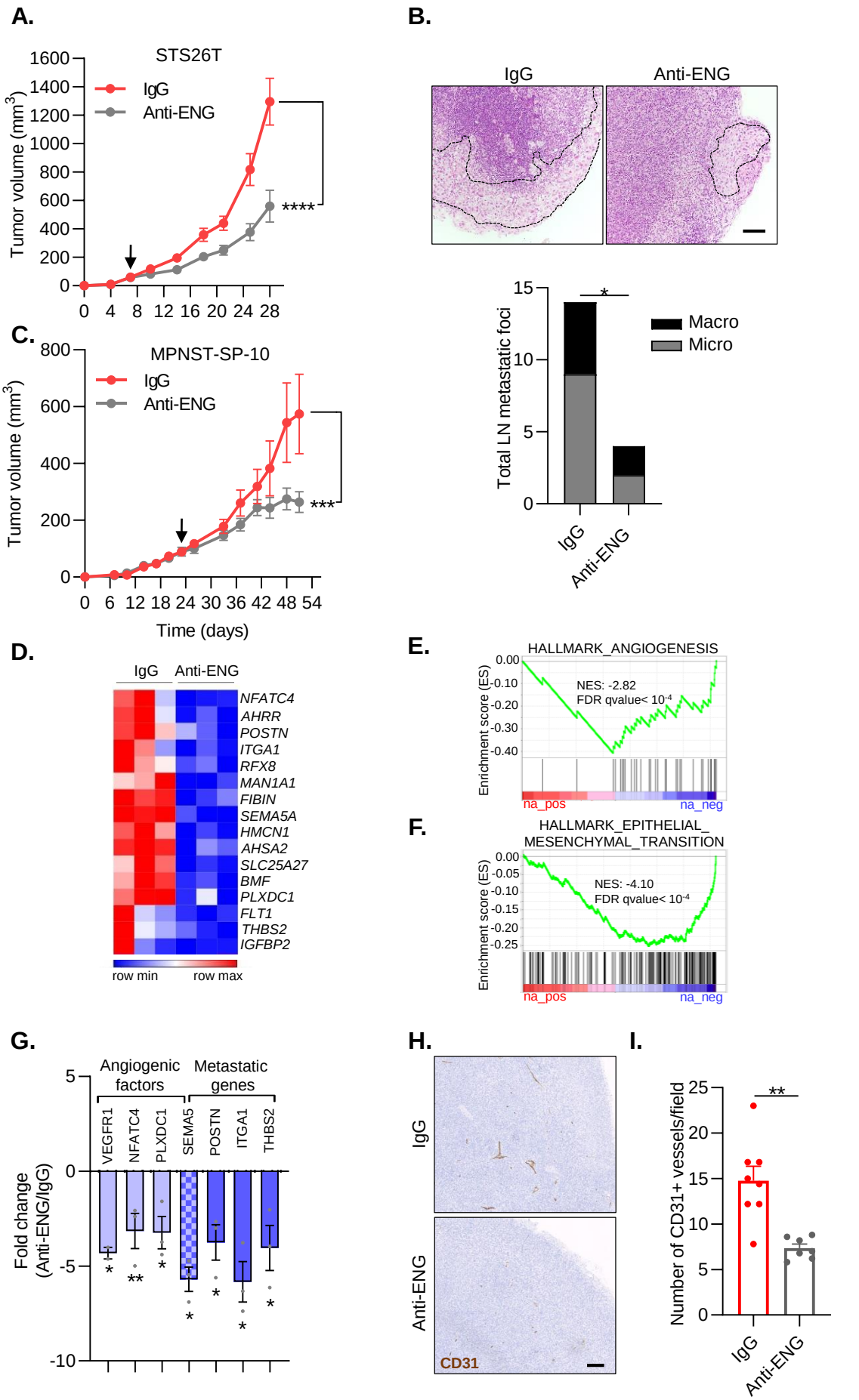
A.
STS26T
IgG
Anti-ENG
Tumor volume (mm3)
1600
1400
1200
1000
800
600
400
200
0
0 4 8 12 16 20 24 28
****
B.
IgG
Anti-ENG
Total LN metastatic foci
15
10
5
0
*
Macro
Micro
IgG
Anti-ENG
C.
MPNST-SP-10
IgG
Anti-ENG
Tumor volume (mm3)
800
600
400
200
0
0 6 12 18 24 30 36 42 48 54
Time (days)
***
D.
IgG
Anti-ENG
NFATC4
AHRR
POSTN
ITGA1
RFX8
MAN1A1
FIBIN
SEMA5A
HMCN1
AHSA2
SLC25A27
BMF
PLXDC1
FLT1
THBS2
IGFBP2
row min
row max
E.
HALLMARK_ANGIOGENESIS
Enrichment score (ES)
0.00
-0.10
-0.20
-0.30
-0.40
NES: -2.82
FDR qvalue< 10-4
na_pos
na_neg
F.
HALLMARK_EPITHELIAL_
MESENCHYMAL_TRANSITION
Enrichment score (ES)
0.00
-0.05
-0.10
-0.15
-0.20
-0.25
NES: -4.10
FDR qvalue< 10-4
na_pos
na_neg
G.
Angiogenic factors
Metastatic genes
VEGFR1
NFATC4
PLXDC1
SEMA5
POSTN
ITGA1
THBS2
Fold change (Anti-ENG/IgG)
5
0
-5
-10
H.
IgG
Anti-ENG
CD31
I.
Number of CD31+ vessels/field
25
20
15
10
5
0
**
IgG
Anti-ENG

Figure 4

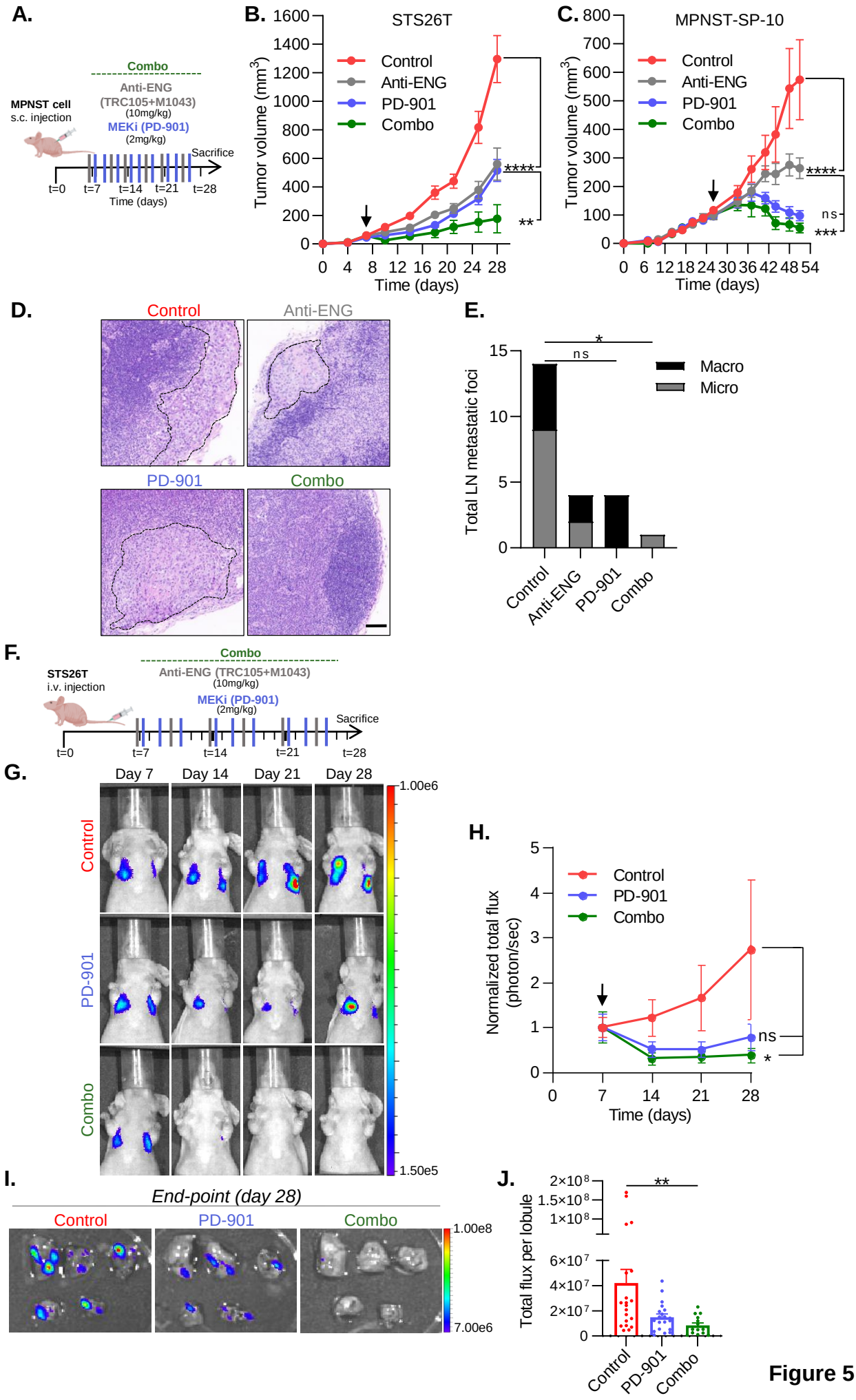
A.
Combo
Anti-ENG
(TRC105+M1043)
(10mg/kg)
MEKi (PD-901)
(2mg/kg)
MPNST cell
s.c. injection
Sacrifice
t=0
t=7
t=14
t=21
t=28
Time (days)
B.
STS26T
Control
Anti-ENG
PD-901
Combo
Tumor volume (mm3)
****
**
Time (days)
C.
MPNST-SP-10
Control
Anti-ENG
PD-901
Combo
Tumor volume (mm3)
****
ns
***
Time (days)
D.
Control
Anti-ENG
PD-901
Combo
E.
Total LN metastatic foci
*
ns
Macro
Micro
Control
Anti-ENG
PD-901
Combo
F.
Combo
STS26T
i.v. injection
Anti-ENG (TRC105+M1043)
(10mg/kg)
MEKi (PD-901)
(2mg/kg)
Sacrifice
t=0
t=7
t=14
t=21
t=28
G.
Day 7
Day 14
Day 21
Day 28
Control
PD-901
Combo
1.00e6
1.50e5
H.
Normalized total flux
(photon/sec)
Control
PD-901
Combo
ns
*
Time (days)
I.
End-point (day 28)
Control
PD-901
Combo
1.00e8
7.00e6
J.
Total flux per lobule
**
Control
PD-901
Combo

Figure 5

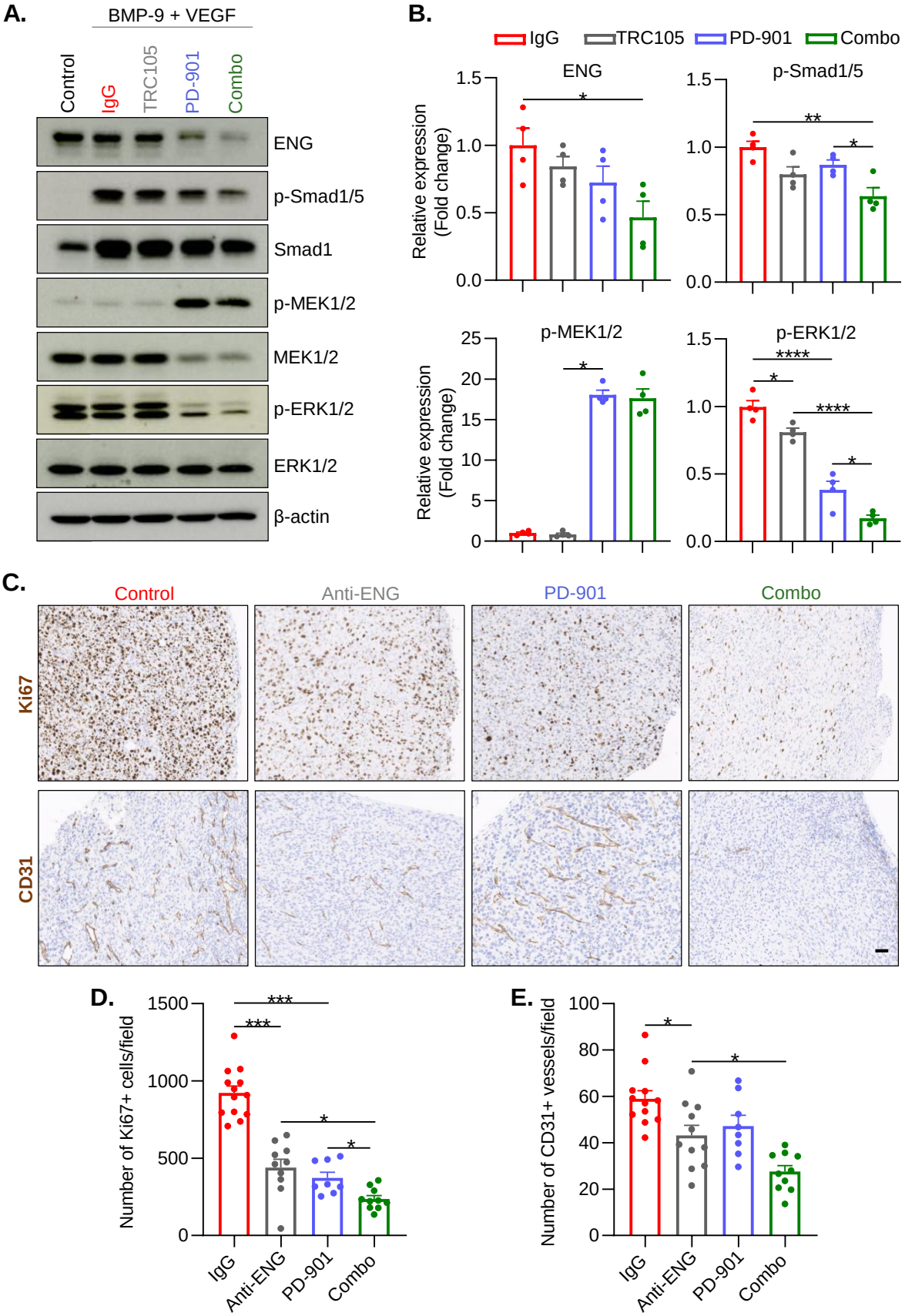
A.
BMP-9 + VEGF
Control
IgG
TRC105
PD-901
Combo
ENG
p-Smad1/5
Smad1
p-MEK1/2
MEK1/2
p-ERK1/2
ERK1/2
β-actin
B.
IgG
TRC105
PD-901
Combo
ENG
p-Smad1/5
p-MEK1/2
p-ERK1/2
Relative expression (Fold change)
C.
Control
Anti-ENG
PD-901
Combo
Ki67
CD31
D.
Number of Ki67+ cells/field
IgG
Anti-ENG
PD-901
Combo
E.
Number of CD31+ vessels/field
IgG
Anti-ENG
PD-901
Combo

Figure 6

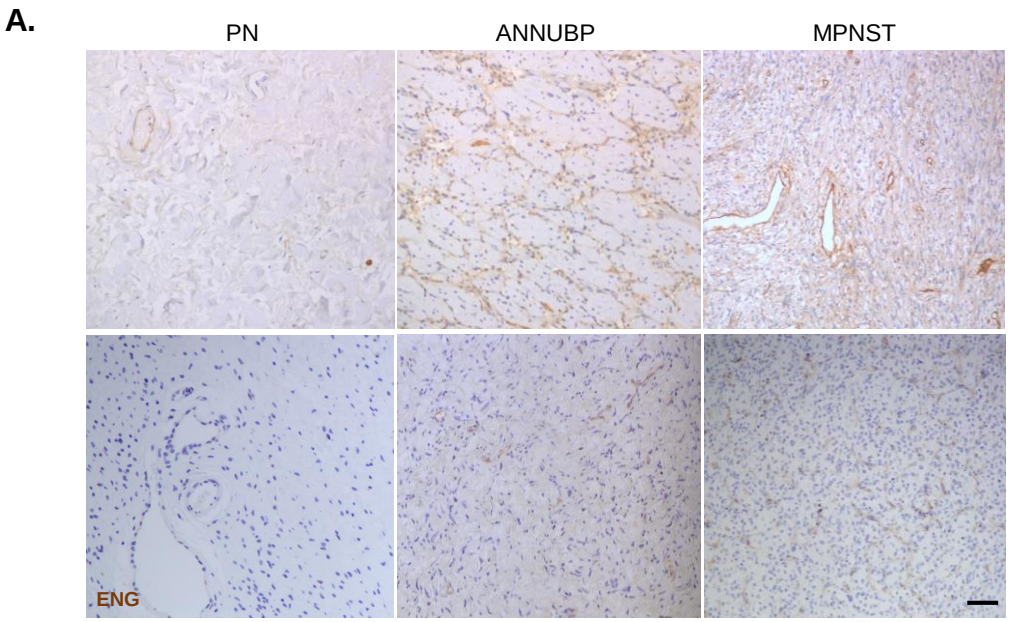

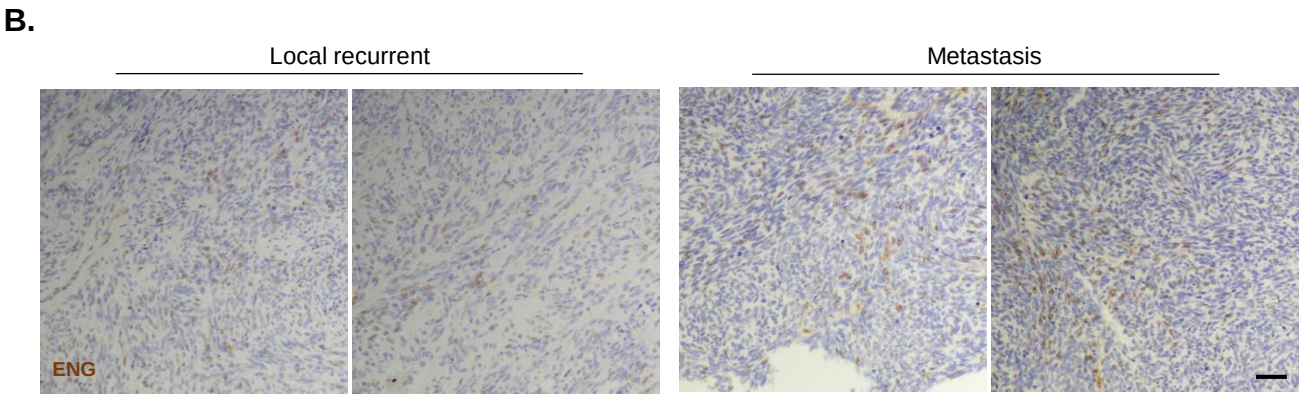

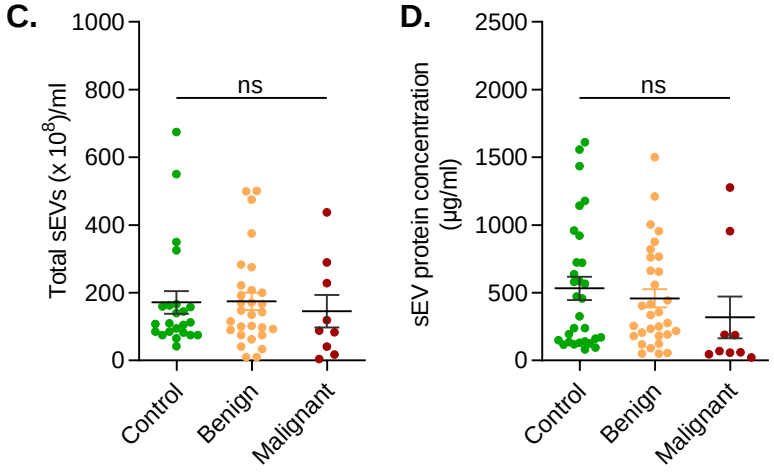

Suppl. Figure 1

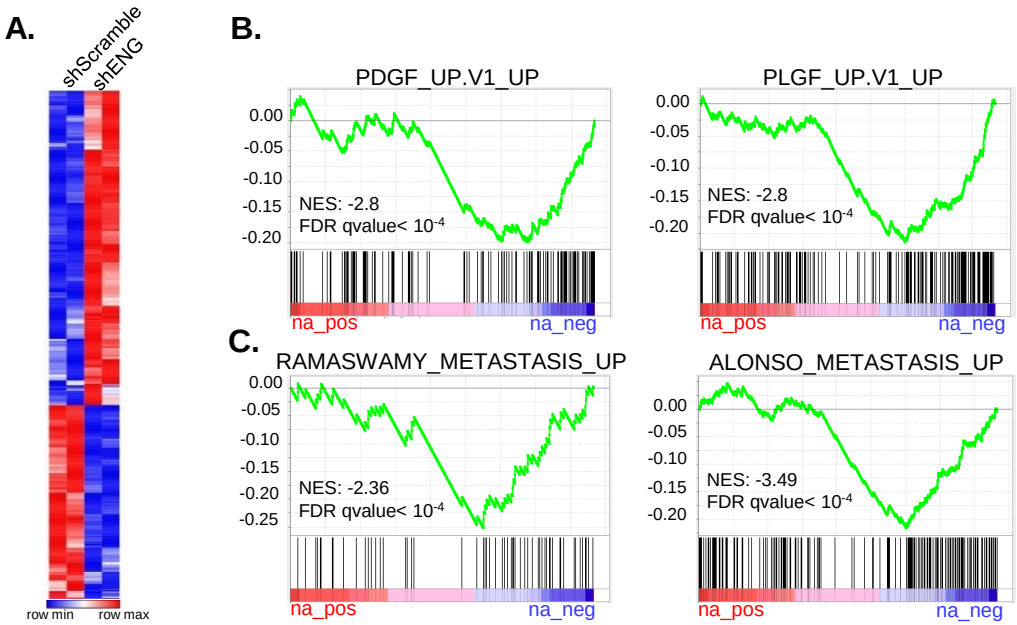

Suppl. Figure 2

A.

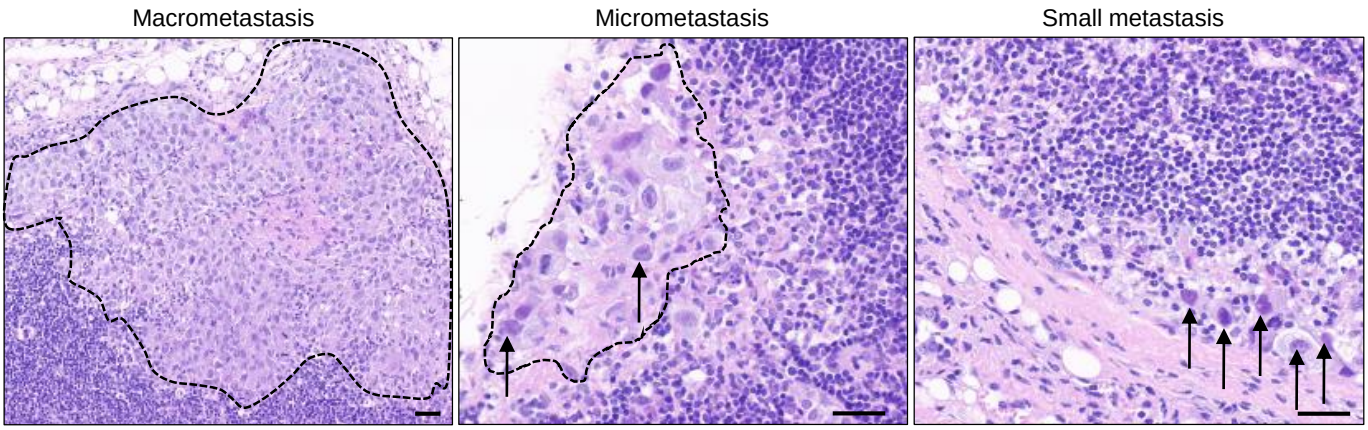

B.

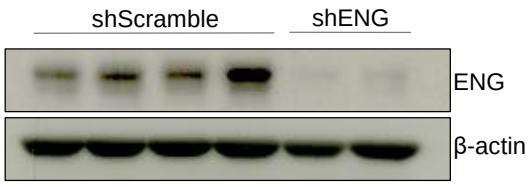

C.

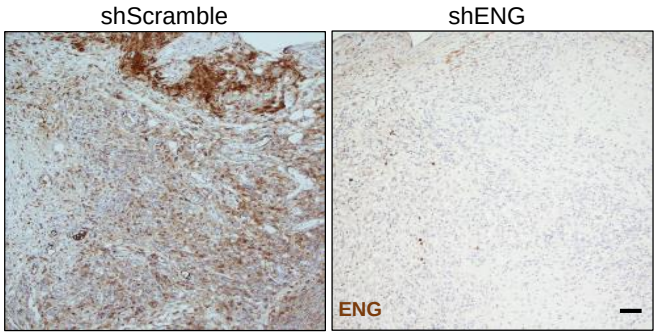

D.

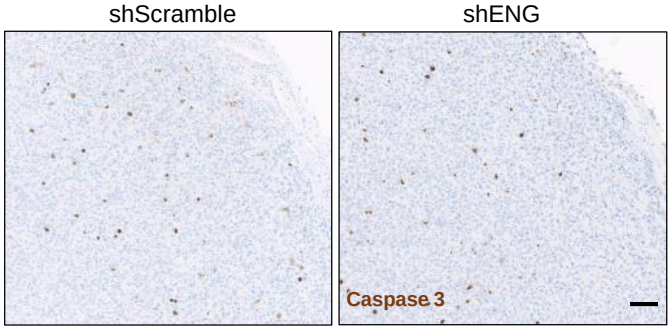

E.

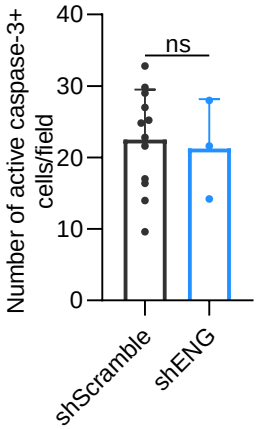

Suppl. Figure 3

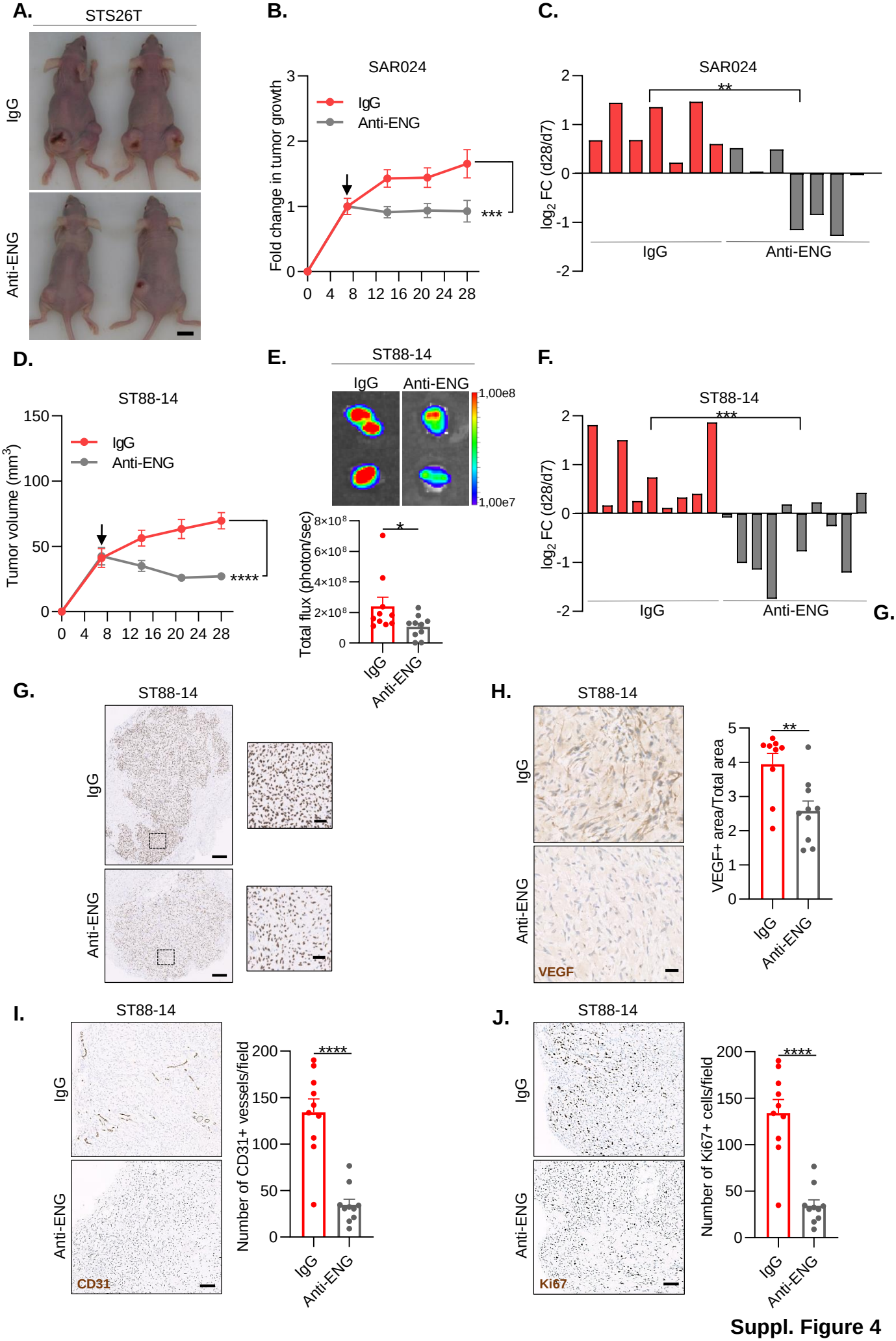

Suppl. Figure 4

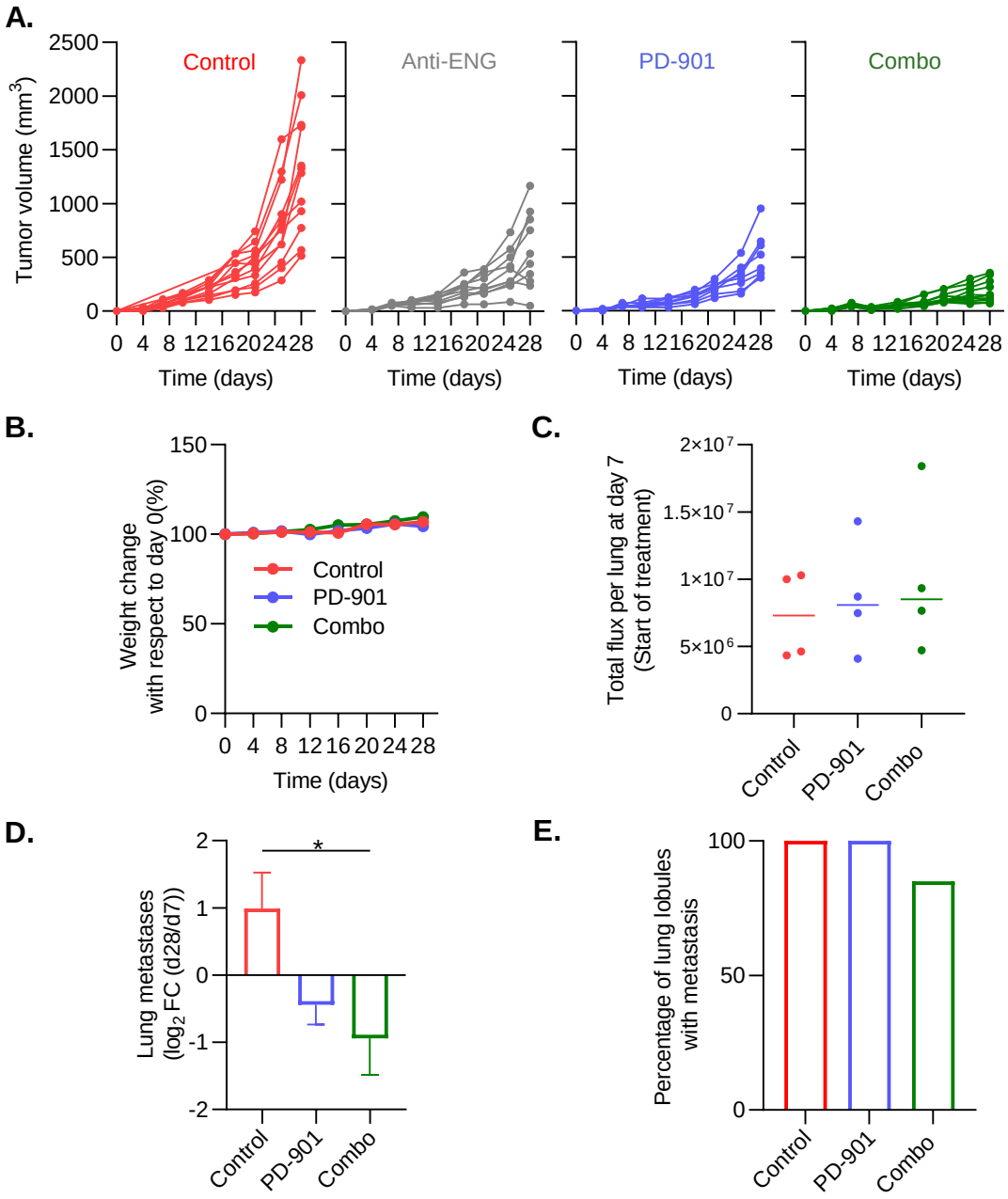

Suppl. Figure 5

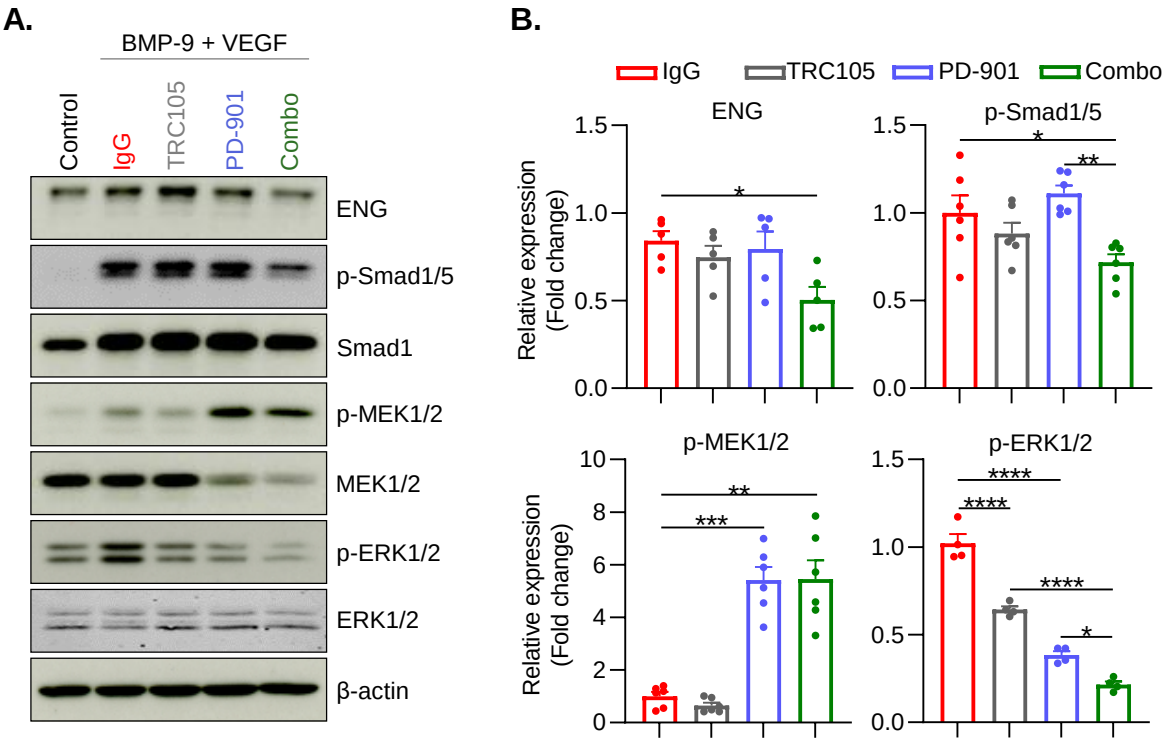

Suppl. Figure 6

Supplementary Table 1. Taqman probes used for quantitative PCR.

Taqman probe	Species	Catalog number	Company
ENG	Human	Hs00923996_m1	Thermo Fisher
FGF1	Human	Hs01092738_m1	Thermo Fisher
FGF2	Human	Hs00266645_m1	Thermo Fisher
HPRT1	Human	Hs02800695_m1	Thermo Fisher
ITGA1	Human	Hs00235006_m1	Thermo Fisher
ITGB1	Human	Hs01127536_m1	Thermo Fisher
NFATC4	Human	Hs00190037_m1	Thermo Fisher
PDGFc	Human	Hs00211916_m1	Thermo Fisher
POSTN	Human	Hs01566750_m1	Thermo Fisher
S100A1	Human	Hs00984741_m1	Thermo Fisher
SEMA5A	Human	Hs01549381_m1	Thermo Fisher
THBS1	Human	Hs00962908_m1	Thermo Fisher
THBS2	Human	Hs01568063_m1	Thermo Fisher
VEGFA	Human	Hs00900055_m1	Thermo Fisher
VEGFc	Human	Hs01099203_m1	Thermo Fisher
VEGFR1	Human	Hs01052961_m1	Thermo Fisher

Supplementary Table 2. Primary antibodies used for immunoblotting and histological analysis.

Antibody	Dilution	Isotype	Company	Catalog number	Use
Anti-CD31	1/100	Rabbit	Abcam	ab28364	IHC
Anti-cleaved caspase-3 (Asp175)	1/400	Rabbit	Cell Signaling Technology	9661	IHC
Anti-endoglin	1/100	Mouse	DAKO	M3527	IHC
Anti-Ki67	1/500	Mouse	DAKO	IR626	IHC
Anti-VEGF (SP28)	Prediluted	Rabbit	Abcam	ab27620	IHC
Anti-endoglin	1/1000	Rabbit	Abcam	ab169545	Western blot
Anti-MEK1/2	1/1000	Rabbit	Cell Signaling Technology	8727	Western blot
Anti-p44/42 MAPK (ERK1/2)	1/1000	Mouse	Cell Signaling Technology	9107	Western blot
Anti-phospho-MEK1/2 (Ser217/221)	1/1000	Rabbit	Cell Signaling Technology	9154	Western blot
Anti-phospho-p44/42 MAPK (Erk1/2) (Thr202/Tyr204)	1/2000	Rabbit	Cell Signaling Technology	9101	Western blot
Anti-phospho-Smad1/5 (Ser463/465)	1/1000	Rabbit	Cell Signaling Technology	9516	Western blot
Anti-Smad1	1/1000	Rabbit	Cell Signaling Technology	6944	Western blot
Anti-β-Actin	1/10000	Mouse	Sigma	A5441	Western blot

Supplementary Table 3. Significant deregulated genes in shENG versus shScramble STS26T cells.

Significant downregulated genes with FDR<0.05				Significant upregulated genes with FDR<0.05			
gene_id	log2(fold_change)	p_value	q_value	gene_id	log2(fold_change)	p_value	q_value
RRS1	-0,402025	0,00325	0,0447129	*GAGE10*	inf	0,00005	0,0020208
DDX39A	-0,40273	0,0036	0,0478718	*COL3A1*	5,55532	0,00155	0,027179
NSUN2	-0,403807	0,0033	0,0452493	*FRZB*	4,07066	0,00025	0,0069566
HIPK2	-0,404276	0,0031	0,0433262	*OLR1*	3,33446	0,0022	0,034285
LAMB3	-0,404292	0,0036	0,0478718	*CD69*	3,27629	0,00005	0,0020208
NUP50	-0,405937	0,00345	0,0464789	*CACNA2D1*	2,94747	0,00045	0,0110281
CALD1	-0,40888	0,0026	0,0382005	*PDPN*	2,84011	0,00005	0,0020208
NMD3	-0,411265	0,00325	0,0447129	*NTF3*	2,49706	0,0001	0,0034822
RBBP8	-0,414051	0,0028	0,0405113	*NEDD9*	2,49192	0,00005	0,0020208
PDGFC	-0,415066	0,00375	0,0491769	*LYPD6B*	2,44955	0,00005	0,0020208
NOP56	-0,415137	0,0026	0,0382005	*HTRA3*	2,43695	0,0002	0,0058561
TBC1D15	-0,41688	0,00335	0,0455297	*ITM2A*	2,35485	0,00195	0,0314629
HMGA1	-0,417565	0,0021	0,0329347	*C10orf81*	2,33206	0,00005	0,0020208
TPM4	-0,418495	0,0023	0,03522	*RNF128*	2,27843	0,0016	0,0275849
C1GALT1	-0,426172	0,00345	0,0464789	*HAVCR2*	1,96353	0,00255	0,0378265
NUCKS1	-0,42626	0,00165	0,0281711	*SLC1A1*	1,94621	0,00005	0,0020208
RANBP1	-0,427203	0,0018	0,0297834	*ALX4*	1,92689	0,00005	0,0020208
PARP4	-0,42754	0,0016	0,0275849	*MEST*	1,91905	0,00005	0,0020208
IFRD1	-0,427852	0,0025	0,0372642	*PPP1R14C*	1,79874	0,00145	0,0259422
NQO1	-0,428478	0,0018	0,0297834	*ROPN1L*	1,77264	0,00305	0,0431162
METAP2	-0,429423	0,0014	0,0252307	*TNF*	1,7428	0,00005	0,0020208
KLHL5	-0,430096	0,0016	0,0275849	*RRAD*	1,73867	0,00005	0,0020208
MAGOHB	-0,431392	0,0038	0,0494642	*SEPT4*	1,67762	0,00115	0,0222195
MOK	-0,433044	0,00285	0,0409463	*MEGF10*	1,66589	0,00005	0,0020208
ENOPH1	-0,433613	0,00225	0,0347131	*RAB26*	1,64682	0,0003	0,0080745
MTMR6	-0,433811	0,00245	0,0366964	*MSC*	1,64627	0,00005	0,0020208
LPXN	-0,433963	0,00155	0,027179	*DAPK1*	1,62904	0,00005	0,0020208
AMIGO2	-0,434198	0,00135	0,0246175	*ADC*	1,61395	0,0008	0,0168287
TMPO	-0,434214	0,00205	0,0323564	*MMP11*	1,61295	0,0029	0,0415195
LTN1	-0,436465	0,00135	0,0246175	*FAM110B*	1,59509	0,00005	0,0020208
LTV1	-0,438948	0,00205	0,0323564	*C10orf10*	1,58769	0,00035	0,0090831
AIMP1	-0,439003	0,00335	0,0455297	*LINC00511*	1,57852	0,0002	0,0058561
PCID2	-0,439232	0,00205	0,0323564	*OASL*	1,57015	0,00005	0,0020208
SRGN	-0,443465	0,0019	0,0308581	*MN1*	1,56848	0,00005	0,0020208
SRGAP1	-0,443937	0,00375	0,0491769	*LRRN4*	1,51814	0,0001	0,0034822
C4orf43	-0,444312	0,0031	0,0433262	*FAP*	1,48392	0,0009	0,0184291
BRIX1	-0,445078	0,00125	0,0234532	*ATF3*	1,47674	0,00005	0,0020208
CWC27	-0,448045	0,00365	0,0484322	*DMRT2*	1,46226	0,00015	0,0046342
ATP8B1	-0,448546	0,00225	0,0347131	*MX2*	1,4575	0,00005	0,0020208
DHX33	-0,451212	0,0017	0,0286674	*KCNK6*	1,43668	0,00005	0,0020208
OTUD4	-0,451258	0,00275	0,0399284	*DNM3OS*	1,43398	0,00005	0,0020208

RALBP1	-0,451391	0,0012	0,022934	*EDN1*	1,41743	0,00005	0,0020208
SLC3A2	-0,451573	0,00095	0,0192927	*CD70*	1,41391	0,00005	0,0020208
SNX24	-0,451956	0,00245	0,0366964	*NXN*	1,3956	0,00005	0,0020208
POLR3F	-0,452388	0,0026	0,0382005	*QPRT*	1,39104	0,0001	0,0034822
AP1AR	-0,452645	0,00255	0,0378265	*IFI44L*	1,3877	0,00005	0,0020208
TTC35	-0,453574	0,0033	0,0452493	*SEL1L3*	1,38693	0,00005	0,0020208
SLC25A43	-0,456343	0,00265	0,0387044	*PAEP*	1,38646	0,0035	0,0468962
HSPA13	-0,456586	0,0011	0,0214892	*CD24*	1,38104	0,00005	0,0020208
USP12	-0,456749	0,00125	0,0234532	*VGLL2*	1,37401	0,00005	0,0020208
ARPC5	-0,45676	0,0007	0,0155476	*ACCN2*	1,37108	0,00005	0,0020208
C3orf64	-0,457743	0,00385	0,0497995	*LOC100216546*	1,36982	0,00005	0,0020208
PIK3CB	-0,457747	0,00195	0,0314629	*LOC728643*	1,36962	0,0001	0,0034822
STK39	-0,459103	0,00135	0,0246175	*ATP6V0D2*	1,35347	0,0021	0,0329347
CDC42EP2	-0,459591	0,0037	0,0488852	*TCN1*	1,3522	0,0007	0,0155476
RFWD3	-0,460625	0,0008	0,0168287	*CTXN1*	1,35153	0,00375	0,0491769
GPBP1L1	-0,461638	0,00115	0,0222195	*DACT1*	1,35091	0,00005	0,0020208
CKAP2L	-0,461753	0,00085	0,01761	*EPHA4*	1,34138	0,00005	0,0020208
CCNA2	-0,461795	0,00325	0,0447129	*ATF7IP2*	1,33963	0,00005	0,0020208
CKAP2	-0,463376	0,00125	0,0234532	*GDA*	1,33739	0,00005	0,0020208
SLC35B1	-0,463699	0,0016	0,0275849	*MX1*	1,33136	0,00005	0,0020208
CEP152	-0,464483	0,00195	0,0314629	*SMAD6*	1,32865	0,00285	0,0409463
EID2	-0,466405	0,0034	0,0460064	*PARM1*	1,32684	0,00005	0,0020208
ABCE1	-0,467884	0,0011	0,0214892	*ADORA2A*	1,32382	0,0001	0,0034822
ALPK2	-0,468313	0,00245	0,0366964	*TMEM45A*	1,32205	0,00005	0,0020208
KAT6A	-0,469631	0,0017	0,0286674	*TMCC2*	1,29607	0,00025	0,0069566
KIAA0020	-0,471201	0,00065	0,014729	*L1CAM*	1,28724	0,00005	0,0020208
SLC7A11	-0,472017	0,00135	0,0246175	*GJA3*	1,28696	0,00005	0,0020208
CD55	-0,473335	0,0014	0,0252307	*EPHB6*	1,28044	0,00005	0,0020208
SAMD4A	-0,473802	0,0017	0,0286674	*SEMA3B*	1,2761	0,00335	0,0455297
PHLDA2	-0,473883	0,0015	0,0267204	*ACSS1*	1,27432	0,00005	0,0020208
PAK1IP1	-0,473911	0,00045	0,0110281	*JUP*	1,26302	0,00005	0,0020208
EIF1B	-0,474092	0,00215	0,0335482	*DPP4*	1,25922	0,00005	0,0020208
DCAF12	-0,475468	0,00085	0,01761	*PCOLCE2*	1,2504	0,00005	0,0020208
MB21D1	-0,477065	0,0025	0,0372642	*MST4*	1,2458	0,00005	0,0020208
BNC1	-0,47721	0,0013	0,0240979	*CHST15*	1,24448	0,00005	0,0020208
HTATSF1	-0,477313	0,0006	0,0138506	*MFAP2*	1,24406	0,00005	0,0020208
VEGFA	-0,477687	0,0006	0,0138506	*OR7E12P*	1,23558	0,00145	0,0259422
FGF2	-0,478081	0,00335	0,0455297	*S1PR2*	1,23359	0,0007	0,0155476
RRP15	-0,479768	0,00075	0,0163344	*ANKLE1*	1,21269	0,00005	0,0020208
RELB	-0,481054	0,00315	0,0437275	*HLA-DOB*	1,21213	0,00165	0,0281711
B4GALT6	-0,482487	0,0032	0,0442721	*LOC728392*	1,21135	0,00175	0,0291911
MTR	-0,482521	0,0005	0,0119448	*MAP3K8*	1,20986	0,00025	0,0069566
STYX	-0,482776	0,0016	0,0275849	*TOX*	1,2067	0,00015	0,0046342
MIDN	-0,482981	0,0016	0,0275849	*FHL1*	1,20324	0,00005	0,0020208
PLAUR	-0,483451	0,0006	0,0138506	*ABHD15*	1,20177	0,00005	0,0020208
TRIM11	-0,48433	0,002	0,0318527	*DISP2*	1,20008	0,00005	0,0020208

HMGB2	-0,485531	0,00035	0,0090831	*KIAA1161*	1,19572	0,00005	0,0020208
FOSL2	-0,486825	0,00125	0,0234532	*CCL2*	1,19479	0,00005	0,0020208
NANP	-0,487564	0,00185	0,0302453	*GLIPR2*	1,19073	0,00005	0,0020208
THUMPD1	-0,488479	0,00105	0,0208428	*NID2*	1,18391	0,00005	0,0020208
TRMU	-0,489099	0,00145	0,0259422	*IFI27*	1,17282	0,00005	0,0020208
TIPIN	-0,489552	0,0012	0,022934	*ZNF558*	1,17244	0,0021	0,0329347
LOC339290	-0,490448	0,00285	0,0409463	*ANK1*	1,17191	0,00005	0,0020208
MND1	-0,490894	0,002	0,0318527	*CYBRD1*	1,16883	0,00005	0,0020208
CENPC1	-0,491527	0,00205	0,0323564	*TNFSF10*	1,16662	0,00005	0,0020208
ELP3	-0,491756	0,0016	0,0275849	*HSPA12A*	1,16254	0,00005	0,0020208
KBTBD2	-0,492355	0,0006	0,0138506	*ZNF518B*	1,16054	0,00005	0,0020208
IGFN1	-0,492748	0,0017	0,0286674	*HBE1*	1,15152	0,0001	0,0034822
UAP1	-0,492893	0,00055	0,0129386	*PTGS1*	1,15142	0,00005	0,0020208
C9orf5	-0,492937	0,0008	0,0168287	*LLGL2*	1,14963	0,00005	0,0020208
TMEM192	-0,493273	0,00095	0,0192927	*FNDC4*	1,14283	0,0008	0,0168287
ANXA3	-0,494004	0,0001	0,0034822	*DMD*	1,1424	0,00005	0,0020208
KLHL2	-0,494232	0,00105	0,0208428	*PCOLCE*	1,13644	0,00005	0,0020208
FAM214B	-0,495518	0,00315	0,0437275	*GFRA1*	1,13572	0,00005	0,0020208
TMPRSS15	-0,499394	0,00025	0,0069566	*TPTEP1*	1,13304	0,00005	0,0020208
C1orf55	-0,500018	0,0012	0,022934	*RASD2*	1,1297	0,0035	0,0468962
ODC1	-0,501895	0,00015	0,0046342	*COL5A2*	1,12699	0,00005	0,0020208
ZNF146	-0,501981	0,00045	0,0110281	*LOC100129534*	1,12642	0,0036	0,0478718
NEDD4	-0,503029	0,0003	0,0080745	*HAPLN3*	1,11777	0,00005	0,0020208
CEP170	-0,503162	0,00065	0,014729	*RTN2*	1,1105	0,0002	0,0058561
YEATS4	-0,503376	0,001	0,0200765	*C3*	1,10938	0,00005	0,0020208
SLC39A10	-0,503987	0,0013	0,0240979	*CGN*	1,1054	0,00005	0,0020208
ZMYND11	-0,505068	0,00015	0,0046342	*FLNC*	1,10488	0,00005	0,0020208
LOC647979	-0,505249	0,00015	0,0046342	*RGAG4*	1,10445	0,00005	0,0020208
OSTF1	-0,507809	0,00155	0,027179	*NBR2*	1,10036	0,00065	0,014729
C9orf41	-0,508483	0,0036	0,0478718	*SLC25A42*	1,09818	0,00005	0,0020208
TRAPPC6B	-0,508688	0,0008	0,0168287	*ATP7B*	1,09587	0,00005	0,0020208
ECHS1	-0,508786	0,0002	0,0058561	*PADI1*	1,09559	0,00035	0,0090831
ZBTB11	-0,509407	0,0008	0,0168287	*FLRT3*	1,09331	0,0011	0,0214892
TAF1A	-0,509749	0,0014	0,0252307	*TM7SF2*	1,09135	0,00005	0,0020208
TAF4B	-0,510818	0,0027	0,0393415	*MT1F*	1,08225	0,00005	0,0020208
ANKRD50	-0,511292	0,0003	0,0080745	*IRF9*	1,07796	0,00005	0,0020208
RAD1	-0,513242	0,0001	0,0034822	*ARHGEF16*	1,07172	0,00005	0,0020208
CD274	-0,5134	0,00075	0,0163344	*NTNG1*	1,068	0,0008	0,0168287
CDKN2D	-0,513612	0,0008	0,0168287	*LOC158257*	1,06594	0,00315	0,0437275
MCL1	-0,51379	0,0002	0,0058561	*ELOVL2*	1,06074	0,00005	0,0020208
C4orf32	-0,514591	0,00235	0,0357194	*GATSL3*	1,05802	0,00035	0,0090831
PPAT	-0,517092	0,0005	0,0119448	*OAS1*	1,05527	0,0001	0,0034822
APOO	-0,517559	0,00085	0,01761	*CITED2*	1,05475	0,00005	0,0020208
LRRCC1	-0,520571	0,00305	0,0431162	*C14orf45*	1,05157	0,0037	0,0488852
TICAM1	-0,520672	0,00125	0,0234532	*SLC16A13*	1,04915	0,00015	0,0046342
ZNF215	-0,520865	0,00105	0,0208428	*PGM2L1*	1,04578	0,00005	0,0020208

BTG3	-0,521179	0,0002	0,0058561	*C1orf226*	1,04527	0,00005	0,0020208
BARD1	-0,52167	0,0013	0,0240979	*MMP13*	1,04331	0,00005	0,0020208
ZNF263	-0,521922	0,00065	0,014729	*EGR1*	1,04254	0,00005	0,0020208
MAPK6	-0,522579	0,00015	0,0046342	*PTGER4*	1,04197	0,00005	0,0020208
PIM3	-0,524814	0,0008	0,0168287	*HAVCR1*	1,03919	0,00005	0,0020208
HCFC2	-0,524918	0,00245	0,0366964	*FLRT2*	1,03747	0,00005	0,0020208
DLX1	-0,525215	0,003	0,042654	*CCDC69*	1,03441	0,00005	0,0020208
SETD7	-0,525436	0,00025	0,0069566	*STRA6*	1,03152	0,00005	0,0020208
MLF1IP	-0,525951	0,0005	0,0119448	*ADAMTS15*	1,03137	0,00005	0,0020208
UTP15	-0,527159	0,00065	0,014729	*MYO1D*	1,02944	0,00005	0,0020208
ZNF639	-0,528955	0,0001	0,0034822	*KSR1*	1,02351	0,00005	0,0020208
LAPTM5	-0,530008	0,00105	0,0208428	*EPS8L2*	1,02045	0,00005	0,0020208
IPMK	-0,530018	0,0017	0,0286674	*EFEMP1*	1,01861	0,00005	0,0020208
ZNF480	-0,530283	0,00075	0,0163344	*CYP2S1*	1,01717	0,0026	0,0382005
ATP2B1	-0,531563	0,00025	0,0069566	*ABCA7*	1,01715	0,00005	0,0020208
MZT1	-0,531712	0,00025	0,0069566	*PLEKHN1*	1,01565	0,00045	0,0110281
TMEM64	-0,532238	0,0016	0,0275849	*NRP2*	1,01542	0,00005	0,0020208
LOC654433	-0,532566	0,0035	0,0468962	*PROS1*	1,01502	0,00005	0,0020208
NUFIP2	-0,532716	0,00015	0,0046342	*CEND1*	1,01046	0,00015	0,0046342
APOOL	-0,533166	0,0008	0,0168287	*HCAR1*	1,00954	0,0001	0,0034822
C16orf52	-0,534958	0,00145	0,0259422	*C4orf39*	1,00355	0,0028	0,0405113
ADCY7	-0,535459	0,00075	0,0163344	*EPHB4*	1,00178	0,00005	0,0020208
ENOX2	-0,537164	0,0003	0,0080745	*C16orf5*	1,00124	0,00005	0,0020208
EMP1	-0,537795	0,00015	0,0046342	*FAM26E*	0,997622	0,0035	0,0468962
C5orf30	-0,538682	0,00105	0,0208428	*GPRC5C*	0,994511	0,00005	0,0020208
MYPN	-0,538805	0,0005	0,0119448	*KIAA1377*	0,993647	0,00005	0,0020208
CTNNAL1	-0,541541	0,00005	0,0020208	*NFKBIA*	0,992022	0,00005	0,0020208
FOXG1	-0,544485	0,00165	0,0281711	*SULF2*	0,991979	0,00005	0,0020208
RAB11FIP2	-0,545164	0,00045	0,0110281	*KIAA1522*	0,990938	0,00005	0,0020208
VDAC1	-0,545173	0,00005	0,0020208	*LOX*	0,988421	0,00005	0,0020208
HIPK3	-0,546634	0,00065	0,014729	*FADS2*	0,985181	0,00005	0,0020208
FBXO5	-0,547454	0,00005	0,0020208	*ANGPTL2*	0,982146	0,0038	0,0494642
PAICS	-0,548993	0,00005	0,0020208	*KLK6*	0,980555	0,00175	0,0291911
ZSCAN12	-0,549833	0,00045	0,0110281	*FLT1*	0,974282	0,00315	0,0437275
LOC96610	-0,553876	0,0012	0,022934	*BEND4*	0,973206	0,00005	0,0020208
GAS2L3	-0,554316	0,0006	0,0138506	*RGS2*	0,971297	0,00005	0,0020208
DYRK3	-0,556283	0,0008	0,0168287	*TNFRSF11B*	0,970647	0,00005	0,0020208
ZNF200	-0,556835	0,0009	0,0184291	*SLC12A8*	0,970483	0,00005	0,0020208
ZNF569	-0,558395	0,0012	0,022934	*FLJ35776*	0,970105	0,0007	0,0155476
FANCE	-0,5595	0,0011	0,0214892	*FSTL3*	0,969224	0,00005	0,0020208
NT5E	-0,562342	0,00005	0,0020208	*ORAI3*	0,968759	0,00005	0,0020208
ZNF594	-0,56543	0,0035	0,0468962	*PLXND1*	0,96424	0,00005	0,0020208
USPL1	-0,565642	0,0005	0,0119448	*CDKN2B*	0,961905	0,00005	0,0020208
ESF1	-0,566095	0,00015	0,0046342	*DNAJA4*	0,956248	0,00005	0,0020208
KCTD6	-0,569812	0,0009	0,0184291	*PIGZ*	0,954459	0,00155	0,027179
RAP2A	-0,570467	0,0001	0,0034822	*IFIT1*	0,95437	0,00005	0,0020208

RNF219	-0,571393	0,00015	0,0046342	*NUAK2*	0,954029	0,00005	0,0020208
COL13A1	-0,571786	0,0001	0,0034822	*TNIK*	0,949488	0,0001	0,0034822
NLRP3	-0,572243	0,00355	0,047463	*MMP15*	0,947835	0,00005	0,0020208
SNAPC1	-0,572556	0,0001	0,0034822	*NFKBIZ*	0,946708	0,00365	0,0484322
CHIC2	-0,574807	0,00095	0,0192927	*VAT1L*	0,946266	0,00005	0,0020208
ACOX2	-0,575541	0,00115	0,0222195	*CCDC74A*	0,94527	0,0004	0,0102299
HIPK1	-0,575579	0,00005	0,0020208	*PLAT*	0,945029	0,00005	0,0020208
TRIM35	-0,578298	0,0002	0,0058561	*LOC644656*	0,94501	0,001	0,0200765
AOX1	-0,57847	0,0005	0,0119448	*PNRC1*	0,943581	0,00005	0,0020208
SGPP1	-0,578602	0,00035	0,0090831	*RNF157*	0,93453	0,00005	0,0020208
C20orf20	-0,579904	0,0002	0,0058561	*KIAA1199*	0,934263	0,00005	0,0020208
CCDC86	-0,581538	0,0001	0,0034822	*C1QTNF6*	0,925221	0,00005	0,0020208
SH3BGRL	-0,58279	0,00115	0,0222195	*PIK3C2B*	0,922999	0,00005	0,0020208
STC1	-0,584731	0,00005	0,0020208	*SLC27A3*	0,922069	0,0014	0,0252307
CD83	-0,586305	0,00055	0,0129386	*F2RL3*	0,921599	0,0004	0,0102299
FABP5	-0,590115	0,00015	0,0046342	*CEBPD*	0,9215	0,00005	0,0020208
FOXD1	-0,590617	0,00025	0,0069566	*FRMD4B*	0,918715	0,0003	0,0080745
ZNF238	-0,591079	0,00005	0,0020208	*OLFML2B*	0,917698	0,00045	0,0110281
PLK3	-0,591081	0,00285	0,0409463	*ST3GAL5*	0,915494	0,0002	0,0058561
SERTAD2	-0,591285	0,00025	0,0069566	*SARDH*	0,914989	0,0007	0,0155476
SLC14A1	-0,592411	0,00005	0,0020208	*SIPA1L2*	0,905433	0,00005	0,0020208
NGF	-0,593004	0,00325	0,0447129	*LAMA5*	0,905411	0,00005	0,0020208
PPP1R18	-0,593244	0,00005	0,0020208	*PLCXD3*	0,90278	0,00005	0,0020208
ARHGAP11A	-0,5939	0,00005	0,0020208	*SAMD9L*	0,898386	0,00005	0,0020208
SEPSECS	-0,59445	0,00165	0,0281711	*EFNA1*	0,897991	0,00005	0,0020208
GRPEL2	-0,596629	0,00005	0,0020208	*OLFML2A*	0,897126	0,00005	0,0020208
B3GNT2	-0,598998	0,0004	0,0102299	*AFAP1L2*	0,895768	0,00005	0,0020208
LIG4	-0,600285	0,00015	0,0046342	*P2RX6*	0,892677	0,0023	0,03522
TIPARP	-0,601487	0,00005	0,0020208	*TTC30B*	0,891944	0,0001	0,0034822
RFK	-0,602759	0,00015	0,0046342	*IFIT2*	0,891136	0,00005	0,0020208
KLHL8	-0,603394	0,00015	0,0046342	*XAF1*	0,891027	0,0001	0,0034822
SPRY4	-0,6043	0,0008	0,0168287	*ADORA1*	0,890877	0,00005	0,0020208
GAN	-0,605681	0,00385	0,0497995	*DIXDC1*	0,889782	0,00005	0,0020208
ZNF449	-0,608649	0,002	0,0318527	*CKB*	0,888798	0,0003	0,0080745
FAM107B	-0,609737	0,00005	0,0020208	*SPIRE2*	0,886971	0,0003	0,0080745
ZNF193	-0,610344	0,00135	0,0246175	*LOC100505817*	0,885195	0,0038	0,0494642
SDR42E1	-0,61041	0,00005	0,0020208	*VAV3*	0,883698	0,00025	0,0069566
FAM19A2	-0,610507	0,00385	0,0497995	*LOC338799*	0,881079	0,00025	0,0069566
GDNF	-0,613449	0,0024	0,0363004	*TNFAIP3*	0,880285	0,00005	0,0020208
SLC25A25	-0,613659	0,0002	0,0058561	*ACTBL2*	0,880116	0,00025	0,0069566
KLF2	-0,614886	0,0031	0,0433262	*C1orf150*	0,878426	0,00215	0,0335482
RAB28	-0,616773	0,00085	0,01761	*BST2*	0,876649	0,00035	0,0090831
CCDC80	-0,617191	0,00195	0,0314629	*ZNF699*	0,872294	0,00005	0,0020208
TOMM5	-0,617543	0,00005	0,0020208	*CREB3L1*	0,869981	0,00005	0,0020208
MESDC1	-0,619472	0,00055	0,0129386	*CELSR2*	0,869969	0,00005	0,0020208
SLC16A7	-0,620804	0,0016	0,0275849	*PHLDB3*	0,868578	0,00255	0,0378265

FASTKD3	-0,622938	0,0009	0,0184291	*C9orf116*	0,866336	0,00185	0,0302453
ZNF574	-0,623047	0,0001	0,0034822	*COLEC12*	0,865556	0,00005	0,0020208
SDHAP1	-0,62382	0,0026	0,0382005	*PFKFB4*	0,864875	0,00005	0,0020208
CPOX	-0,624004	0,0001	0,0034822	*LOC388692*	0,86243	0,00005	0,0020208
CYB5R2	-0,625257	0,00025	0,0069566	*LYPD3*	0,861664	0,00005	0,0020208
PURA	-0,626812	0,00015	0,0046342	*LFNG*	0,858647	0,00005	0,0020208
ZC3H12C	-0,627602	0,00015	0,0046342	*BTN3A3*	0,854065	0,0001	0,0034822
DNTTIP2	-0,629697	0,00005	0,0020208	*LOC401320*	0,851318	0,0006	0,0138506
GATA2	-0,629758	0,0002	0,0058561	*CAPN5*	0,846613	0,0013	0,0240979
PHLDA1	-0,630369	0,00005	0,0020208	*TSPAN9*	0,843268	0,00005	0,0020208
PCNA	-0,631689	0,00005	0,0020208	*LINC00263*	0,842922	0,0001	0,0034822
MME	-0,633617	0,0001	0,0034822	*IL6*	0,838836	0,00005	0,0020208
IER2	-0,634675	0,00005	0,0020208	*ARID5B*	0,837534	0,00005	0,0020208
TUSC1	-0,636045	0,0017	0,0286674	*C1QTNF1*	0,837016	0,00005	0,0020208
KLF10	-0,636567	0,0001	0,0034822	*ITGB8*	0,836953	0,00005	0,0020208
PPM1A	-0,637182	0,00005	0,0020208	*IFITM1*	0,832526	0,00025	0,0069566
ZNF468	-0,640243	0,00085	0,01761	*TRIM47*	0,830099	0,0002	0,0058561
PAK3	-0,642398	0,0008	0,0168287	*OAS2*	0,828118	0,00005	0,0020208
ZBTB41	-0,644682	0,0001	0,0034822	*PBXIP1*	0,82619	0,00005	0,0020208
MYEF2	-0,645647	0,0001	0,0034822	*PDGFB*	0,82573	0,0018	0,0297834
ANTXR2	-0,645748	0,00045	0,0110281	*KIAA1462*	0,824774	0,00005	0,0020208
LARP1B	-0,647659	0,00005	0,0020208	*DCDC2*	0,82451	0,00005	0,0020208
OSGIN1	-0,64997	0,002	0,0318527	*CELSR1*	0,819071	0,00005	0,0020208
C10orf88	-0,656521	0,00015	0,0046342	*MCTP2*	0,817509	0,00015	0,0046342
EREG	-0,656595	0,00005	0,0020208	*TTC39B*	0,815689	0,0012	0,022934
TEF	-0,658856	0,00045	0,0110281	*HDAC11*	0,815385	0,00005	0,0020208
SLC7A5	-0,659516	0,00005	0,0020208	*KLHDC8B*	0,814821	0,0009	0,0184291
TOB1	-0,660487	0,0008	0,0168287	*PTPRR*	0,813598	0,0003	0,0080745
ZNF778	-0,661073	0,0008	0,0168287	*ARHGAP27*	0,81314	0,00055	0,0129386
IKZF5	-0,661075	0,0003	0,0080745	*GREM1*	0,813006	0,0025	0,0372642
IKBKAP	-0,666457	0,00005	0,0020208	*TBX15*	0,812911	0,0023	0,03522
CCP110	-0,667226	0,00005	0,0020208	*IGFBP4*	0,810172	0,00005	0,0020208
OTUD6B	-0,668851	0,00005	0,0020208	*FOXO4*	0,809687	0,0001	0,0034822
E2F3	-0,668973	0,00005	0,0020208	*DEM1*	0,806983	0,0001	0,0034822
FZD8	-0,67295	0,00005	0,0020208	*TRANK1*	0,806431	0,00005	0,0020208
SIX4	-0,673508	0,00035	0,0090831	*CPT1C*	0,804683	0,0005	0,0119448
STARD13	-0,673525	0,00005	0,0020208	*TRIB1*	0,804411	0,00005	0,0020208
PER3	-0,67455	0,00005	0,0020208	*LRRC17*	0,804304	0,00005	0,0020208
SOX7	-0,676699	0,00095	0,0192927	*GALM*	0,803713	0,0013	0,0240979
BIRC3	-0,677246	0,00015	0,0046342	*PDGFRL*	0,803422	0,0003	0,0080745
ZFP28	-0,679069	0,00155	0,027179	*APCDD1L*	0,802631	0,00015	0,0046342
BRIP1	-0,680538	0,00005	0,0020208	*IRF5*	0,800979	0,00055	0,0129386
PLD6	-0,681915	0,0018	0,0297834	*ASPHD1*	0,793191	0,00175	0,0291911
DSP	-0,683775	0,0005	0,0119448	*GMIP*	0,790526	0,00005	0,0020208
ZNF25	-0,689656	0,00165	0,0281711	*HOOK2*	0,787177	0,00125	0,0234532
E2F8	-0,689938	0,00005	0,0020208	*MMP17*	0,786766	0,0001	0,0034822

ZNF225	-0,691769	0,00075	0,0163344	*OCEL1*	0,784171	0,00175	0,0291911
ZNF48	-0,697531	0,0009	0,0184291	*TMEM102*	0,782004	0,0004	0,0102299
FNDC3A	-0,701742	0,00005	0,0020208	*HKDC1*	0,780515	0,0002	0,0058561
KLHL11	-0,708176	0,001	0,0200765	*TCEA2*	0,77964	0,00005	0,0020208
RP9	-0,714125	0,00005	0,0020208	*P4HA2*	0,775162	0,00005	0,0020208
PRKRIR	-0,71881	0,00005	0,0020208	*MRAS*	0,77293	0,00005	0,0020208
LY6K	-0,719025	0,00225	0,0347131	*MLLT3*	0,766703	0,00045	0,0110281
EIF4E3	-0,719114	0,00125	0,0234532	*KAZN*	0,766644	0,00005	0,0020208
IL11	-0,720887	0,00005	0,0020208	*ESRG*	0,766149	0,00005	0,0020208
AMMECR1	-0,722746	0,00005	0,0020208	*SLC12A7*	0,765738	0,00005	0,0020208
ACAT1	-0,72499	0,00005	0,0020208	*TFEB*	0,76511	0,00035	0,0090831
SLCO1B3	-0,730744	0,00005	0,0020208	*CDKL5*	0,764787	0,00305	0,0431162
TMEM156	-0,733133	0,00005	0,0020208	*AQP1*	0,76382	0,0023	0,03522
SLC16A6	-0,737165	0,0038	0,0494642	*BMP1*	0,761682	0,00005	0,0020208
C16orf87	-0,750425	0,00015	0,0046342	*HTR1D*	0,758551	0,0031	0,0433262
ZBTB34	-0,751044	0,00005	0,0020208	*ZNF385A*	0,757727	0,0006	0,0138506
AMMECR1L	-0,751639	0,00005	0,0020208	*OPLAH*	0,755303	0,00115	0,0222195
MPP4	-0,752626	0,00015	0,0046342	*SERPINA5*	0,754788	0,00015	0,0046342
NEDD4L	-0,754432	0,00005	0,0020208	*SAMD12*	0,751991	0,001	0,0200765
PAWR	-0,755428	0,00005	0,0020208	*CEP112*	0,751966	0,00005	0,0020208
FOSL1	-0,756129	0,00005	0,0020208	*SLC6A9*	0,75169	0,0005	0,0119448
IER5L	-0,761831	0,0001	0,0034822	*CMBL*	0,751025	0,00015	0,0046342
ICK	-0,764573	0,00005	0,0020208	*TMEM180*	0,749977	0,00265	0,0387044
NAV3	-0,76676	0,00005	0,0020208	*DUSP1*	0,74995	0,00045	0,0110281
PHF13	-0,773246	0,00005	0,0020208	*BCL6*	0,749421	0,0003	0,0080745
ATG5	-0,776269	0,00005	0,0020208	*PDE4A*	0,745509	0,00025	0,0069566
ARPP19	-0,77685	0,00005	0,0020208	*LIPG*	0,745368	0,00005	0,0020208
NGFR	-0,780093	0,00075	0,0163344	*FSTL5*	0,744759	0,0001	0,0034822
ZFP161	-0,781813	0,00005	0,0020208	*IL1R1*	0,743853	0,00005	0,0020208
PCLO	-0,782851	0,00005	0,0020208	*LOC100216545*	0,738878	0,0015	0,0267204
AKAP2	-0,783839	0,00045	0,0110281	*LOC100134868*	0,733604	0,0031	0,0433262
LPAR1	-0,784205	0,00005	0,0020208	*GPRC5B*	0,73313	0,00005	0,0020208
SERTAD3	-0,796963	0,00005	0,0020208	*GCHFR*	0,732137	0,0002	0,0058561
FBXL3	-0,798612	0,00005	0,0020208	*TMEM150A*	0,731729	0,0031	0,0433262
SMEK3P	-0,80854	0,00155	0,027179	*IPW*	0,730649	0,00305	0,0431162
WDR66	-0,812562	0,00005	0,0020208	*PODXL*	0,729693	0,00005	0,0020208
FAM217B	-0,814979	0,00005	0,0020208	*C12orf76*	0,729139	0,00125	0,0234532
EIF5A2	-0,816666	0,00005	0,0020208	*COL5A1*	0,728969	0,00005	0,0020208
G0S2	-0,817454	0,00005	0,0020208	*KLF7*	0,725666	0,00015	0,0046342
FOXN2	-0,821378	0,00005	0,0020208	*LIMCH1*	0,725652	0,00005	0,0020208
SP140	-0,821707	0,00075	0,0163344	*SGK1*	0,725198	0,00005	0,0020208
TOB2	-0,821945	0,00005	0,0020208	*CARD11*	0,723832	0,00005	0,0020208
MYBL1	-0,827161	0,00005	0,0020208	*TGFBR3*	0,722841	0,0002	0,0058561
ZNF28	-0,828912	0,00005	0,0020208	*TRIM55*	0,721464	0,00055	0,0129386
KBTBD6	-0,831279	0,00005	0,0020208	*MEIS3P1*	0,720186	0,0007	0,0155476
FAM129A	-0,834196	0,00005	0,0020208	*ARHGAP28*	0,717551	0,00025	0,0069566

ZNF503	-0,841376	0,0019	0,0308581	*SCD*	0,715663	0,00005	0,0020208
RNF182	-0,842747	0,00005	0,0020208	*AMOT*	0,713352	0,00035	0,0090831
C10orf116	-0,855357	0,00005	0,0020208	*GSN*	0,711755	0,00005	0,0020208
CMAS	-0,857667	0,00005	0,0020208	*PDGFRB*	0,711485	0,00005	0,0020208
ZNF420	-0,863728	0,0001	0,0034822	*SLC16A4*	0,710767	0,0029	0,0415195
HDAC9	-0,868619	0,00005	0,0020208	*FAM84B*	0,710351	0,00015	0,0046342
DUSP7	-0,876892	0,00005	0,0020208	*ADRA1B*	0,709578	0,00045	0,0110281
RIMS2	-0,887637	0,00005	0,0020208	*BMF*	0,70784	0,00065	0,014729
ZFP1	-0,889958	0,00005	0,0020208	*EMR1*	0,707545	0,00015	0,0046342
C15orf48	-0,895805	0,0016	0,0275849	*CTGF*	0,707486	0,00005	0,0020208
MARS2	-0,906693	0,00005	0,0020208	*PTK2B*	0,706778	0,0006	0,0138506
AGPAT9	-0,912283	0,00005	0,0020208	*SSC5D*	0,70499	0,0029	0,0415195
EP400NL	-0,939007	0,0038	0,0494642	*TMEM133*	0,701853	0,0005	0,0119448
NCEH1	-0,954155	0,00005	0,0020208	*TUBA1A*	0,699037	0,00005	0,0020208
ZNF597	-0,960546	0,00015	0,0046342	*CYR61*	0,69844	0,00005	0,0020208
FAM111B	-0,963671	0,00005	0,0020208	*MPP2*	0,697969	0,0008	0,0168287
LOC730755	-0,964413	0,00005	0,0020208	*TSPAN15*	0,69756	0,0001	0,0034822
FAIM3	-0,971537	0,0001	0,0034822	*PCYOX1L*	0,694634	0,0011	0,0214892
ZNF823	-0,986551	0,00005	0,0020208	*UST*	0,693904	0,00045	0,0110281
ZNF280B	-0,993097	0,00005	0,0020208	*SLC17A5*	0,692916	0,00035	0,0090831
ZNF567	-0,997861	0,00005	0,0020208	*C20orf194*	0,691467	0,00005	0,0020208
CASP3	-1,00203	0,00005	0,0020208	*CCDC28B*	0,688197	0,001	0,0200765
CHAC1	-1,00638	0,00005	0,0020208	*SPATA6*	0,687835	0,0007	0,0155476
C1orf51	-1,02297	0,00005	0,0020208	*PHLDA3*	0,687444	0,0005	0,0119448
VSTM1	-1,03846	0,00235	0,0357194	*AMIGO1*	0,685297	0,00185	0,0302453
FBP1	-1,07474	0,00005	0,0020208	*ZHX2*	0,682297	0,00015	0,0046342
C1D	-1,13799	0,00005	0,0020208	*C7orf41*	0,681842	0,0002	0,0058561
RFX8	-1,14714	0,0005	0,0119448	*MAPK8IP1*	0,680245	0,0003	0,0080745
ID3	-1,14741	0,00005	0,0020208	*CXXC5*	0,678605	0,0031	0,0433262
HBEGF	-1,14966	0,00005	0,0020208	*S100A4*	0,678402	0,0001	0,0034822
ZNF284	-1,16963	0,00025	0,0069566	*SFXN5*	0,675574	0,00005	0,0020208
FGF1	-1,18761	0,00005	0,0020208	*LOC642852*	0,674756	0,00005	0,0020208
ELAVL2	-1,20743	0,00015	0,0046342	*PTPRU*	0,673851	0,00015	0,0046342
WDR69	-1,2133	0,00095	0,0192927	*IFIT3*	0,673804	0,00005	0,0020208
ID1	-1,25149	0,00005	0,0020208	*PLD1*	0,672128	0,00005	0,0020208
ELTD1	-1,31285	0,00005	0,0020208	*C14orf79*	0,670503	0,00115	0,0222195
ZIC2	-1,31393	0,0001	0,0034822	*ZC3H12A*	0,666468	0,00015	0,0046342
DDIT4	-1,34204	0,00005	0,0020208	*SECTM1*	0,665869	0,0005	0,0119448
MCTP1	-1,34927	0,00005	0,0020208	*ARHGEF4*	0,665636	0,00045	0,0110281
FAM196B	-1,3671	0,0008	0,0168287	*HES6*	0,665277	0,00235	0,0357194
TMEM71	-1,39905	0,00185	0,0302453	*MARCKSL1*	0,663539	0,00005	0,0020208
MAPRE1	-1,4727	0,00005	0,0020208	*SH3TC1*	0,663152	0,0037	0,0488852
ZC4H2	-1,53739	0,00015	0,0046342	*CERCAM*	0,663087	0,0001	0,0034822
RAB3A	-1,71738	0,00245	0,0366964	*DOCK2*	0,661981	0,00055	0,0129386
IL24	-1,78881	0,00005	0,0020208	*STK32C*	0,659796	0,00135	0,0246175
ENG	-1,82974	0,00005	0,0020208	*HSPA1A*	0,659154	0,00005	0,0020208

BCHE	-1,83949	0,00005	0,0020208	*ENPP2*	0,656472	0,0026	0,0382005
				SYTL2	0,656097	0,0003	0,0080745
				TMEM117	0,65333	0,00125	0,0234532
				TOR2A	0,652236	0,00175	0,0291911
				SLC43A2	0,652176	0,0014	0,0252307
				LTBP4	0,650338	0,0001	0,0034822
				TCF7	0,650305	0,0002	0,0058561
				F11R	0,648507	0,00005	0,0020208
				STARD10	0,647517	0,0016	0,0275849
				PBX1	0,647303	0,00135	0,0246175
				DHCR7	0,646911	0,00005	0,0020208
				ZNF608	0,642555	0,00005	0,0020208
				FBLN1	0,639585	0,00075	0,0163344
				PRUNE2	0,635067	0,00015	0,0046342
				SERPINH1	0,633986	0,00005	0,0020208
				SLC17A9	0,633931	0,0002	0,0058561
				SORBS1	0,633466	0,00035	0,0090831
				ATP11A	0,63318	0,00005	0,0020208
				LMBR1L	0,633087	0,0007	0,0155476
				DNAJB4	0,632285	0,00025	0,0069566
				CLCN6	0,631135	0,00265	0,0387044
				SPTBN2	0,630873	0,0001	0,0034822
				TBC1D8B	0,629742	0,0036	0,0478718
				SGK223	0,62652	0,00065	0,014729
				MGC21881	0,626379	0,00195	0,0314629
				MT1E	0,626244	0,00245	0,0366964
				LOC730091	0,624143	0,00135	0,0246175
				ALDOC	0,623111	0,0014	0,0252307
				REPS2	0,619134	0,00005	0,0020208
				DAB2IP	0,618554	0,0024	0,0363004
				TRIM45	0,617788	0,0032	0,0442721
				KCNN4	0,615265	0,00035	0,0090831
				S100A3	0,61345	0,0013	0,0240979
				MAGEC1	0,610999	0,0001	0,0034822
				CLDN11	0,609337	0,00125	0,0234532
				CLIP2	0,608263	0,0002	0,0058561
				EHHADH	0,607899	0,00175	0,0291911
				TMEM51	0,607494	0,00235	0,0357194
				NACC2	0,607213	0,00015	0,0046342
				CNTNAP1	0,606691	0,00125	0,0234532
				NRBP2	0,605679	0,002	0,0318527
				PAFAH2	0,605666	0,00105	0,0208428
				GNAO1	0,604954	0,00235	0,0357194
				LYST	0,60269	0,0001	0,0034822
				SLC46A3	0,602654	0,00105	0,0208428
				ENGASE	0,602469	0,0003	0,0080745

PAPSS2	0,601647	0,0004	0,0102299
NAT14	0,600317	0,00015	0,0046342
ITGA11	0,599077	0,0018	0,0297834
FGF13	0,598549	0,0021	0,0329347
SPOCK1	0,597633	0,00005	0,0020208
SIX5	0,597283	0,00055	0,0129386
DNAJC4	0,596928	0,00375	0,0491769
SERINC2	0,596136	0,00065	0,014729
MSMO1	0,595909	0,00005	0,0020208
SCG2	0,594692	0,00005	0,0020208
SLAMF7	0,594334	0,0037	0,0488852
ULK1	0,594104	0,0007	0,0155476
BANP	0,594073	0,0021	0,0329347
MIB2	0,590308	0,00135	0,0246175
SDK1	0,589995	0,00015	0,0046342
GALK1	0,589609	0,0004	0,0102299
UBA7	0,585748	0,0011	0,0214892
SMAD7	0,582941	0,0017	0,0286674
ITPK1	0,582387	0,00005	0,0020208
MFI2	0,582236	0,00015	0,0046342
PDE5A	0,579855	0,00255	0,0378265
NRN1	0,579628	0,0024	0,0363004
PXDN	0,577053	0,00005	0,0020208
PITPNM1	0,576676	0,00015	0,0046342
ADA	0,576557	0,00235	0,0357194
GPX3	0,576266	0,0031	0,0433262
PACS1	0,575491	0,0001	0,0034822
WEE1	0,575471	0,0001	0,0034822
ING4	0,575411	0,00015	0,0046342
NDRG4	0,573399	0,00155	0,027179
TMEM67	0,573032	0,0014	0,0252307
TGFB1	0,573008	0,0001	0,0034822
CSMD2	0,572483	0,0006	0,0138506
GPR126	0,571105	0,00005	0,0020208
GBP2	0,57032	0,0002	0,0058561
FAM101B	0,56979	0,00045	0,0110281
CPA4	0,569611	0,00005	0,0020208
IGSF3	0,569525	0,0001	0,0034822
SAMD9	0,567444	0,0001	0,0034822
ALDH4A1	0,566538	0,00205	0,0323564
RELN	0,564474	0,0001	0,0034822
PSD4	0,562674	0,0038	0,0494642
LOC149773	0,562606	0,001	0,0200765
FN1	0,561304	0,00005	0,0020208
MAP3K5	0,559286	0,00035	0,0090831
NFIA	0,558447	0,0017	0,0286674

NLGN2	0,558063	0,00075	0,0163344
SHROOM2	0,556375	0,00335	0,0455297
HLA-H	0,556271	0,00205	0,0323564
BBS9	0,555281	0,00185	0,0302453
F2RL1	0,555037	0,0002	0,0058561
ARL14	0,553091	0,00205	0,0323564
FBXL19	0,55235	0,0008	0,0168287
PLCE1	0,552115	0,00155	0,027179
ZBTB47	0,551074	0,0018	0,0297834
AR	0,550895	0,0007	0,0155476
LEPREL2	0,550372	0,0023	0,03522
SLC25A23	0,548493	0,0015	0,0267204
ARHGEF3	0,548368	0,00085	0,01761
RGS14	0,546641	0,0019	0,0308581
PTGFRN	0,545229	0,00005	0,0020208
SDC3	0,544645	0,00015	0,0046342
CADM1	0,54391	0,00005	0,0020208
COL4A5	0,542728	0,0001	0,0034822
NES	0,541675	0,00035	0,0090831
TNFRSF19	0,541367	0,00065	0,014729
INHBA	0,539967	0,00035	0,0090831
RNF170	0,538548	0,0025	0,0372642
TTYH3	0,537671	0,00005	0,0020208
SPPL2B	0,536946	0,0016	0,0275849
ECE1	0,536042	0,0002	0,0058561
PGPEP1	0,534644	0,002	0,0318527
MOV10	0,533849	0,00045	0,0110281
KRT15	0,533397	0,0034	0,0460064
SEPT6	0,531732	0,00085	0,01761
GABARAPL1	0,530454	0,002	0,0318527
PLXNB1	0,529604	0,00115	0,0222195
NME3	0,529235	0,00345	0,0464789
DHCR24	0,528934	0,00015	0,0046342
FAM53B	0,52867	0,0011	0,0214892
BTN3A2	0,527383	0,00285	0,0409463
COL7A1	0,527118	0,00025	0,0069566
CCDC71L	0,526121	0,00025	0,0069566
NAPRT1	0,525646	0,0026	0,0382005
NCOA7	0,525442	0,00145	0,0259422
DHRS1	0,523833	0,002	0,0318527
DRAM1	0,523308	0,0011	0,0214892
PPP1R3B	0,522109	0,0017	0,0286674
CALHM2	0,519141	0,00225	0,0347131
NCOA1	0,516824	0,0009	0,0184291
HMGCS1	0,516263	0,00025	0,0069566
PARP10	0,51491	0,00325	0,0447129

ACBD7	0,514442	0,0034	0,0460064
TNFRSF9	0,514026	0,0006	0,0138506
ATP13A2	0,513556	0,00085	0,01761
PAM	0,513254	0,00035	0,0090831
TRIM65	0,513089	0,00135	0,0246175
STAT2	0,511835	0,00175	0,0291911
DYNC2H1	0,511744	0,00045	0,0110281
RHBDF1	0,510146	0,00275	0,0399284
GRAMD3	0,510126	0,00075	0,0163344
ERCC6	0,509823	0,00305	0,0431162
FASN	0,509754	0,00015	0,0046342
CD82	0,509528	0,00185	0,0302453
SOX12	0,506634	0,00225	0,0347131
COL12A1	0,50468	0,00025	0,0069566
COL1A1	0,502341	0,00035	0,0090831
COL6A1	0,501612	0,0001	0,0034822
PKP3	0,501603	0,00165	0,0281711
IRF2BPL	0,501149	0,00245	0,0366964
DDR1	0,500018	0,0013	0,0240979
ITFG3	0,499301	0,00295	0,0421375
LEPREL1	0,498574	0,0004	0,0102299
OSBPL1A	0,497609	0,00085	0,01761
CLSTN3	0,493989	0,00335	0,0455297
MAN2A1	0,49314	0,0007	0,0155476
NNMT	0,489529	0,001	0,0200765
STK38	0,488102	0,0012	0,022934
SORT1	0,486343	0,0003	0,0080745
PDLIM1	0,48523	0,00045	0,0110281
SFMBT2	0,485199	0,002	0,0318527
BHLHE41	0,485181	0,00185	0,0302453
MFGE8	0,483693	0,00125	0,0234532
TK2	0,483536	0,00375	0,0491769
CTSF	0,483462	0,0013	0,0240979
GBP1	0,483342	0,0011	0,0214892
CRISPLD2	0,479977	0,00185	0,0302453
CDK14	0,479969	0,00275	0,0399284
DBN1	0,479949	0,0011	0,0214892
SPARC	0,47884	0,00045	0,0110281
LPCAT1	0,478356	0,00175	0,0291911
C14orf133	0,47784	0,0024	0,0363004
UBE2L6	0,475137	0,00355	0,047463
TIMP4	0,472155	0,0019	0,0308581
LIMK1	0,471827	0,00045	0,0110281
DPCD	0,47165	0,0034	0,0460064
FBN1	0,468055	0,00075	0,0163344
PCYT2	0,467324	0,00155	0,027179

SNX18	0,466642	0,00315	0,0437275
ACAP3	0,466193	0,00375	0,0491769
CYBA	0,466045	0,00295	0,0421375
WNT5A	0,46602	0,003	0,042654
PCYOX1	0,464592	0,00135	0,0246175
RAB3B	0,46261	0,00225	0,0347131
SEMA4B	0,462369	0,00215	0,0335482
SIPA1	0,46231	0,0014	0,0252307
IRF1	0,46219	0,0019	0,0308581
CMTM3	0,460601	0,00285	0,0409463
PEX6	0,460298	0,00225	0,0347131
ODZ2	0,457224	0,003	0,042654
FADS1	0,456257	0,0008	0,0168287
LGALS3	0,454082	0,002	0,0318527
SYT11	0,454026	0,0033	0,0452493
APOL6	0,452472	0,0026	0,0382005
CHPF	0,450628	0,00225	0,0347131
WDTC1	0,448935	0,00345	0,0464789
GADD45A	0,448716	0,00245	0,0366964
PRIC285	0,447563	0,00385	0,0497995
TNK2	0,444762	0,0031	0,0433262
LPIN1	0,442342	0,00155	0,027179
ATG9A	0,440206	0,00185	0,0302453
TNS3	0,439944	0,00165	0,0281711
DPYSL3	0,439748	0,0008	0,0168287
EFHC1	0,433935	0,0038	0,0494642
SPTLC2	0,432986	0,00265	0,0387044
ARMC9	0,432318	0,00385	0,0497995
GRB10	0,432096	0,0028	0,0405113
PLXNB2	0,427026	0,00375	0,0491769
LAMB2	0,42691	0,003	0,042654
JUND	0,422149	0,00315	0,0437275
GABARAP	0,422142	0,00215	0,0335482
F3	0,422083	0,0023	0,03522
KLF6	0,420727	0,00155	0,027179
PLOD1	0,413021	0,00265	0,0387044
IDH1	0,411979	0,0027	0,0393415
MYO18A	0,411127	0,00385	0,0497995
DAG1	0,40933	0,0031	0,0433262
F2R	0,405535	0,0032	0,0442721
PGD	0,399888	0,00335	0,0455297
MARCKS	0,397188	0,00335	0,0455297